Astron. Astrophys. 359, 821–842 (2000)

ASTRONOMY AND ASTROPHYSICS

Multiplicity functions and X-ray emission of clusters and groups versus galaxies and quasars

P. Valageas and R. Schaeffer

Service de Physique Théorique, CEN Saclay, 91191 Gif-sur-Yvette, France

Received 17 September 1999 / Accepted 26 April 2000

Abstract. We use a unified analytical formulation - developed in previous papers - for the multiplicity functions of clusters and galaxies. This method is free from the cloud-in-cloud problem encountered in earlier approaches and well adapted to the description of the non-linear clustering features. It is especially suited to *simultane ously* describe rich clusters, groups and galaxies, consistently with the hierarchical picture of gravitational clustering, as well as their evolution in time. We find a good agreement with observations for the cluster temperature function and we compare our method with the standard Press-Schechter prescription. We also obtain the main properties of the Sunyaev-Zel'dovich effect (mean and variance). Then, using a simple model for the cluster X-ray luminosity (taking into account entropy considerations), w e obtain the X-ray luminosity distribution of groups and clusters.

Then, using the same formalism we derive the galaxy and quasar multiplicity functions. In particular, we show that the use of the standard Press-Schechter prescription leads to erroneous conclusions at low redshifts while our approach provides a reasonable agreement with observations in a natural fashion because it is able to distinguish galactic halos from groups or clusters. Finally, we derive the contribution of quasars and galaxies to the X-ray counts. Thus, we obtain *a global and consistent picture of the X-ray emissions from all structures*. In particular, we show that future observations (e.g., from AXAF) could provide interesting information on galaxy evolution. Indeed, they will constrain the importance of a possible hot diffuse gaseous phase in galactic halos and they could reveal massive galaxies which are just being formed, through the X-ray emission of their cooling gas.

Key words: galaxies: clusters: general – galaxies: evolution – galaxies: luminosity function, mass function – galaxies: quasars: general – cosmology: large-scale structure of Universe – cosmology: cosmic microwave background

1. Introduction

Clusters of galaxies are the largest virialized objects, characterized by scales which have just entered the non-linear regime. Thus, they are very rare and their number density is very sensitive to the cosmological parameters and to the amplitude of the initial density fluctuations (within the framework of the usual hierarchical scenarios). As a consequence, as proposed by Oukbir & Blanchard (1992) many authors have compared observations with predictions from numerical simulations (e.g., Eke et al. 1996) or analytic approaches (e.g., Oukbir & Blanchard 1997) in order to obtain constraints on $(\Omega_{\rm m}, \Omega_\Lambda)$ and on the initial power-spectrum $P(k)$. However, the cluster temperature - X-ray luminosity relation involves non-gravitational effects since simple scaling laws (Kaiser 1986) recovered by numerical simulations (Eke et al. 1998) that neglect radiative cooling and supernova or quasar feedback disagree with observations. This could be due to a preheating of the IGM by QSOs or supernovae (Valageas & Silk 1999b; Cavaliere et al. 1997; Ponman et al. 1999) which has not been considered yet by numerical simulations. Thus, analytic approaches are still needed in order to describe clusters. Moreover, they explicitly show the connection of cluster characteristics (e.g., their mass function) with other features of the universe (e.g., various properties of the underlying density field, of galaxies or quasars).

The standard way to estimate the mass multiplicity function of collapsed objects by analytical means, is the well-known Press-Schechter (1974) approximation - hereafter PS - that directly recognizes in the initial, linear, fluctuations of the density field the overdensities that will eventually collapse. This approximation, however, suffers from many drawbacks. One is that it is customary -and necessary in order to bring the analytical form in agreement with numerical simulations- to multiply the result by an ad-hoc factor of two. This cannot be justified by the standard excursion sets argument for realistic filters like the top-hat in real-space as shown in Valageas & Schaeffer (1997) - hereafter VS - (see also Peacock & Heavens 1990). Indeed, in such a case the excursion sets imply a renormalization factor which goes to unity at large masses.

Another fundamental problem, inherently related to hierarchical clustering, is to describe objects embedded within other, less dense but nevertheless virialized, objects, that is to describe *subclustering*. This has long been known (Bardeen et al. 1986) not to be reliable within approaches directly based on recognition of the linear overdensities that will form objects, and is called the *cloud-in-cloud problem*. Indeed, an approach based on counting overdensities in the linear regime leads to severe

overcounting, so severe that the same objects are erroneously counted an infinite number of times (VS). Thus, to describe a universe made of dense galaxies (10^4 times the mean density), as well as of galaxy clusters (10^2 times the mean density), is out of reach of such approaches, while the description of intermediate objects such as Lyα clouds, that may even have densities below the mean, is unthinkable within this framework. Indeed, note that the PS approximation can only deal with just-virialized halos.

Recent progress (VS) in the description of the non-linear density field, through a *non-linear scaling model* based on earlier approaches (Schaeffer 1984, 1985; Balian & Schaeffer 1989; Bernardeau & Schaeffer 1991), with an understanding of its relation to the initial spectrum of fluctuations, leads to analytical expressions that enable one to *directly count the overdensities in the actual non-linear density field*. The result exhibits many analogies with the PS approximation, but it gives a correct normalization and it also solves the cloud-in-cloud problem (there are no divergences). It also provides the correlations of these objects and the associated bias as compared to the matter distribution (Valageas et al. 2000b; Bernardeau & Schaeffer 1992,1999).

For the purposes of the present paper, the scaling approach gives a clear answer to the following problem. Choose *any* density contrast $\Delta = (\rho - \overline{\rho})/\overline{\rho}$ and define objects as having an inner density contrast larger than this threshold. Then *all* the mass in the universe (except a nonvanishing but negligible fraction in the very underdense regions) lies within such objects, that have a distribution of mass or size given by the theory. The choice of a larger contrast results in a different partition of the same mass into smaller objects, the procedure being valid for arbitrarily large contrasts (with obvious limits at the kpc scale where pressure and angular momentum come into play) as long as one remains in the non-linear regime. This is the way *subclustering* can be properly accounted for. Then, the same theory can simultaneously describe virialized clusters, which have a contrast of $\simeq 200$, as well as galaxies (Valageas & Schaeffer 1999), whose contrast is $\simeq 5000$, embedded or not in the latter objects. The procedure also holds for small density contrasts, even negative, provided one is at scales (in the present universe, for instance, not much above 1 Mpc) where the correlation function is large enough so as to insure one is in the fully non-linear regime. This corresponds to *underdense non-linear objects* embedded in much less dense, nearly void regions. The new feature introduced by the scaling model is that, because one directly works in the non-linear regime, this separation can be done properly. The same procedure applied to future non-linear objects in the linear regime as is done in the PS approach would lead to the above mentioned divergences (VS), which is another indication that defining objects directly in the linear regime, as is done in the latter approach, is unsecure.

The analytical predictions of the scaling model have been checked against numerical simulations (Valageas, Lacey & Schaeffer 2000a) under the most extreme conditions, searching for non-linear objects with density contrasts ranging from values as large as $\Delta = 5000$ down to negative values $\Delta = -0.5$, spanning four orders of magnitude and limited only by the accuracy of the simulations. Thus, this approach provides reasonable results, at least in the above range, allowing us to describe non linear objects and their evolution. These theoretical predictions are also in the line of the findings of Moore et al. (1999a) that resolve some of the structure of dark matter halos in their simulation. As a consequence, the mass functions provided by this approach give, with the same parameters, *a unified description of very different objects*, such as galaxies and quasars (Valageas & Schaeffer 1999), Lyα clouds (Valageas, Schaeffer & Silk 1999), the ionization flux emitted by QSOs (Valageas & Silk 1999a), allowing for a consistent picture of the reheating and the reionization history of the universe (Valageas & Silk 1999a,b). Although this had been checked from the beginning of this series of articles, it remains to be explicitly shown that the same approach, without new parameters, provides the correct cluster multiplicity and its observed evolution with redshift.

Thus, the main goals of this article are to:

- check the predictions for the properties of clusters of an analytic method developed in previous studies which can describe in a consistent way the mass functions of various objects (clusters, galaxies, Lyα clouds, etc.) while making the connection with other properties of the density field (correlation functions, counts-in-cells, etc.).
- evaluate by means of the same method the distortion of the CMB anisotropies induced by these X-ray clusters through the Sunyaev-Zel'dovich effect.
- introduce a simple model which can reproduce the observed temperature - X-ray luminosity relation of groups and clusters.
- use the global scope of our description to compare the X-ray emission provided by clusters, groups, galaxies and quasars. In particular, we show that this requires us to go beyond the standard PS prescription in order to deal with various classes of objects which may not be defined by the usual constant density threshold $\Delta_c(z) \sim 177$.

In Sect. 2, we present the expressions of the multiplicity functions and we compare the PS approach with the scaling model, focussing on the cluster mass function. The temperature function and its evolution with redshift are discussed in Sect. 3 while Sect. 4 is devoted to the implications of our model for the characteristics of the Sunyaev-Zel'dovich effect. Next, in Sect. 5 we present a model for the temperature - X-ray luminosity relation and we derive the cluster X-ray luminosity function. Finally, in Sect. 6 we describe the galaxy and quasar luminosity functions predicted by our model, which allows us to draw a complete picture of the X-ray emission from all structures.

2. Multiplicity functions

2.1. Formalism

We define clusters as halos with a mean density contrast equal to Δ_c, where Δ_c is the density contrast at the time of virialization, at the redshift z we consider, given by the spherical collapse

model. This means that clusters just virialize at the redshift at which we see them. For a critical density universe this density threshold is a constant: $\Delta_c \simeq 177$. Numerical simulations show that this value of the density contrast separates reasonably well the virialized halos from the surrounding material still falling onto the overdensity (Cole & Lacey 1996). This justifies this traditional definition of clusters.

Following the method outlined in VS we shall use two prescriptions to get the comoving mass function of these halos. Firstly, we recall the *scaling model* developed in previous papers, which we apply here to clusters of galaxies. Secondly, we also consider the usual PS approximation for the sake of comparison. Undoubtedly, we have in mind that the former supercedes the latter in the sense that it takes full benefit of the hierarchical clustering picture. The main advantages of this scaling approach are i) to make the link between the mass functions and the counts-in-cells statistics and ii) to provide a very powerful tool which can describe many different mass functions (i.e. defined by various density thresholds) as well as other properties of the non-linear density field.

The scaling model assumes that the many-body correlation functions follow specific scaling laws obtained from the stable-clustering ansatz (see VS for details). Then, we attach to each object a parameter x defined by:

$$x(M,z) = \frac{1+\Delta_c}{\bar{\xi}[R(M,z),z]}, \tag{1}$$

where

$$\bar{\xi}(R) = \int_V \frac{d^3r_1\, d^3r_2}{V^2}\, \xi_2(\mathbf{r}_1,\mathbf{r}_2) \quad \text{with} \quad V = \frac{4}{3}\pi R^3$$

is the average of the two-body correlation function $\xi_2(\mathbf{r}_1,\mathbf{r}_2)$ over a spherical cell of radius R and provides the measure of the typical density fluctuations in such a cell. Thus large x correspond to deep, and small x to shallow potential wells. Then, we write the multiplicity function of these objects, defined by the density threshold Δ_c, as (see VS):

$$\eta(M)\frac{dM}{M} = \frac{\bar{\rho}_0}{M}\, x^2 H(x)\, \frac{dx}{x}, \tag{2}$$

where $\bar{\rho}_0$ is the mean density of the universe at $z = 0$. The scaling function $H(x)$ only depends on the initial spectrum of the density fluctuations and must be obtained from numerical simulations. However, from theoretical arguments (see VS, Bernardeau & Schaeffer 1992 and Balian & Schaeffer 1989) it is expected to follow the asymptotic behaviour:

$$x \ll 1 \;:\; H(x) \propto x^{\omega-2} \quad , \quad x \gg 1 \;:\; H(x) \propto x^{\omega_s-1}\, e^{-x/x_*}$$

with $\omega \simeq 0.5$, $\omega_s \sim -3/2$, $x_* \sim 10$ to 20 and by definition it must satisfy:

$$\int_0^\infty x\, H(x)\, dx = 1. \tag{3}$$

This formulation is directly linked to the statistics of the counts-in-cells which involve a scaling function $h(x)$, related to the probability $P(\Delta,R)$ to have a density contrast Δ in a spherical cell of fixed radius R, that scales as:

$$(1+\Delta)\; P(\Delta,R)\; d\Delta = x^2\; h(x)\frac{dx}{x} \quad , \quad x(\Delta) = \frac{1+\Delta}{\bar{\xi}[R,z]}. \tag{4}$$

This function $h(x)$ is very close to $H(x)$, see VS and Valageas et al. (2000a) for details. The relevance of these scaling functions has been checked using numerical simulations for CDM initial conditions by Bouchet et al. (1991) and, more systematically using power-law initial spectra in Colombi et al. (1997), Munshi et al. (1999) and Valageas et al. (2000a). Here we note that in principle this prescription only applies to the highly non-linear regime ($\bar{\xi} \gtrsim 100$) while clusters correspond to mildly non-linear scales ($\bar{\xi} \sim$ 10–100). Hence the cluster mass functions we obtain may show an accuracy of 10%. Note however that the scaling function we shall use, taken from numerical simulations by Bouchet et al. (1991), was measured in this range of $\bar{\xi}$, and was indeed found to describe clustering at the above accuracy.

On the other hand, the usual PS approximation gives

$$\eta(M)\frac{dM}{M} = \sqrt{\frac{2}{\pi}}\frac{\bar{\rho}_0}{M}\frac{\delta_c}{\sigma}\left|\frac{\mathrm{dln}\sigma}{\mathrm{dln}M}\right| \exp\left[-\frac{\delta_c^2}{2\sigma^2}\right]\frac{dM}{M}, \tag{5}$$

where $\delta_c(z)$ is the present linear density contrast for halos which collapsed at redshift z according to the spherical collapse model. As usual, $\sigma(M)$ is the rms density fluctuation extrapolated by linear theory at $z = 0$ at scale M. Here we multiplied the mass function (5) by the usual empirical factor of 2 so that all the mass is contained in such overdensities.

We can see that *the scaling mass function* (2) *predicts more numerous very massive halos but fewer small objects than the PS mass function* (5). This difference can be directly seen through the scaling function $H(x)$. Indeed, as shown in VS the PS formulation can be translated into the scaling approach in the highly non-linear regime where it leads to a specific scaling function:

$$h_{PS}(x) = \sqrt{\frac{2}{\pi}}\frac{5+n}{6\alpha}x^{\frac{5+n}{6}-2}\exp\left[-x^{(5+n)/3}/(2\alpha^2)\right] \tag{6}$$

where n is the slope of the power-spectrum and $\alpha \simeq 1$. A comparison with the function $h(x)$ directly measured in numerical simulations from counts-in-cells (see VS and Valageas et al. 2000a) shows that the large-mass cutoff of the PS mass function is too sharp while its peak (at masses M_* where $\sigma(M_*) = 1$) is too high. This latter region corresponds to low mass clusters in Fig. 1 and to low temperature objects in Fig. 4 and Fig. 5 below. Note however that at very low masses, corresponding to very small galaxies, the PS mass functions give fewer objects than the scaling prescription as seen in Valageas & Schaeffer (1999).

Since in this article we wish to obtain in a consistent fashion the X-ray emission from all discrete sources: clusters, quasars and galaxies, we also need the multiplicity function of galaxies. As described in Valageas & Schaeffer (1999) we define galaxies by *two* constraints to be satisfied simultaneously: the usual density threshold $\Delta_c(z)$ (as for clusters) *and* a cooling condition which ensures that the gas is able to dissipate its energy and form stars. This implies that galactic halos are defined by a density

contrast $\Delta_{gal}(x,z)$ which depends on the mass of the object. Then, we can still use the expressions (1) and (2) to obtain the galaxy mass function, where the density contrast is now set to $\Delta_{gal}(x,z)$ and depends on x (see VS and Valageas et al. 2000a). Moreover, from the identification (6) we can also consider an "extended PS" prescription to count these halos. We shall use this below in Sect. 6 when we deal with galaxies and quasars.

For the numerical calculations we shall consider two cosmologies. First, we study a critical density universe (SCDM) with $\Omega_{\rm b} = 0.04$, $H_0 = 60\,{\rm km\,s^{-1}}$, $\sigma_8 = 0.5$ and a CDM power-spectrum (Davis et al. 1985). Next, we consider an open CDM universe (OCDM) with $\Omega_{\rm m} = 0.3$, $\Omega_\Lambda = 0$, $\Omega_{\rm b} = 0.03$, $H_0 = 60\,{\rm km\,s^{-1}}$ and $\sigma_8 = 0.77$. These values are those we used in previous articles where we considered the luminosity functions of galaxies (Valageas & Schaeffer 1999), Lyman-α absorbers (Valageas et al. 1999) and reionization by stars and quasars (Valageas & Silk 1999a). Thus, this present study of clusters and groups of galaxies completes our description of structure formation in the universe, so that we obtain a unified model which can describe in a consistent fashion all these objects, from small low-density Lyman-α absorbers up to massive clusters.

Recent CMB observations (e.g., de Bernardis et al. 2000) suggest that the universe is flat. However, for our purposes, a ΛCDM universe with $\Omega_{\rm m} = 0.3$ and $\Omega_\Lambda = 0.7$ should be very close to our OCDM scenario, with a slight modification of the parameters of our astrophysical model for galaxies and clusters. In particular, as seen in Peacock & Dodds (1996) the functional relation between the linear and non-linear power-spectra is the same for the OCDM and ΛCDM (i.e. one simply needs to take into account the variation of the linear growth factor). Moreover, the scaling model which leads to the multiplicity function (2) has been seen to agree with the statistics of the projected density κ along the line of sight obtained from numerical simulations for all three SCDM, OCDM and ΛCDM cosmologies, as shown for instance in Valageas (2000). These results strongly suggest that our approach could also be used for the ΛCDM case. (In a similar fashion, the accuracy of the PS prescription is similar for all three cosmologies).

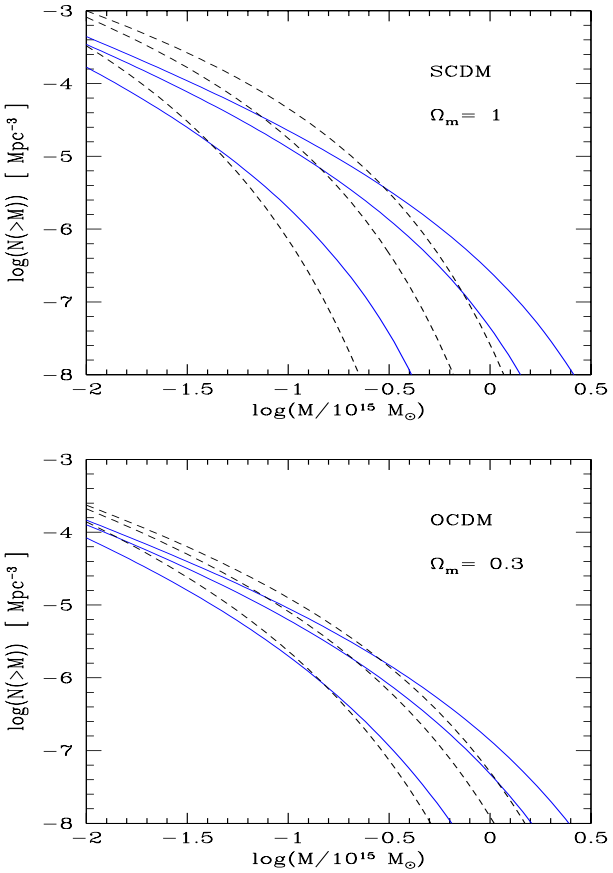

Fig. 1. *Upper panel*: the cluster comoving cumulative mass function at redshifts $z = 0.05,\ z = 0.33$ and $z = 1$, for a critical density universe with a CDM power-spectrum. Higher redshifts lead to fewer massive clusters. The solid lines correspond to the scaling prescription while the dashed lines represent the PS formulation. *Lower panel*: same curves for an open universe with $\Omega_{\rm m} = 0.3$.

2.2. Evolution with redshift of the cluster mass function

We display in Fig. 1 the cluster comoving cumulative mass function we obtain for the two cosmological scenarios we consider in this article, at redshifts $z = 0.05$, $z = 0.33$ and $z = 1$. First, we can check that we recover the trend described in the previous section: the scaling approach predicts fewer low mass halos and more very massive objects than the PS prescription. In a similar fashion, Governato et al. (1999) find that the PS mass function overestimates the number of small clusters ($M < 2\ 10^{14} M_\odot$, for $\sigma_8 = 0.7$) and underestimates the number of massive halos (see also Gross et al. 1998 for a similar trend). However, the discrepancy they measure is smaller than ours. This may be due to the fact that the power-spectrum we use (from Davis et al. 1985) is slightly different from theirs and to the use of our scaling model in a range of $\overline{\xi}$ slightly beyond its range of validity: indeed very high masses correspond to large scales which are getting close to the linear regime where the scaling model is not valid. Nevertheless, the agreement of our predictions (already described in a more general context in VS), with the behaviour observed in the numerical simulations, is quite encouraging.

We can check that the redshift evolution of the mass function is very sensitive to the cosmological parameter $\Omega_{\rm m}$ (e.g., Oukbir & Blanchard 1992; Eke et al. 1996). Indeed, the number of clusters declines faster with z for the critical density universe than for the open model. This is simply due to the fact that in the latter case structures have nearly stopped growing since the redshift where $\Omega_{\rm m}$ became appreciably smaller than unity, whence a very weak evolution with redshift, while in the former case structures keep building under the action of gravity at all epochs.

The dependence on $\Omega_{\rm m}$ of the redshift evolution of the cluster mass function is even more apparent in Fig. 2 which shows the redshift distribution of clusters more massive than $5 \times 10^{14}\ M_\odot$, per square degree, for both SCDM and OCDM scenarios:

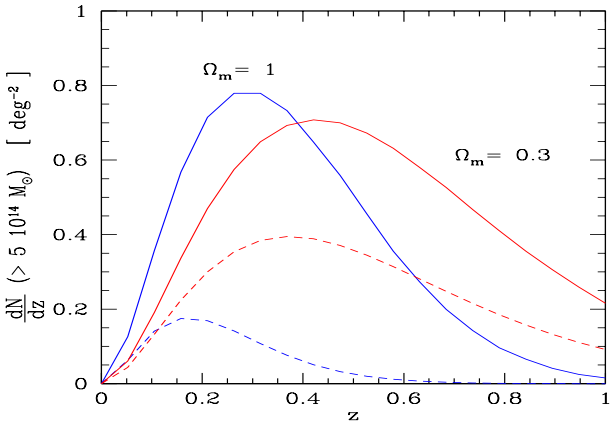

Fig. 2. The redshift distribution per square degree of clusters more massive than $5 \times 10^{14}\ M_\odot$, for $\Omega_{\rm m} = 1$ and $\Omega_{\rm m} = 0.3$. The graph shows the number of clusters $d\mathcal{N}/dz(> 5\ 10^{14}\ M_\odot)$ per unit redshift interval and square degree. The solid lines correspond to the non-linear prescription, while the dashed lines represent the PS formulation. The open universe corresponds to the slowest redshift evolution.

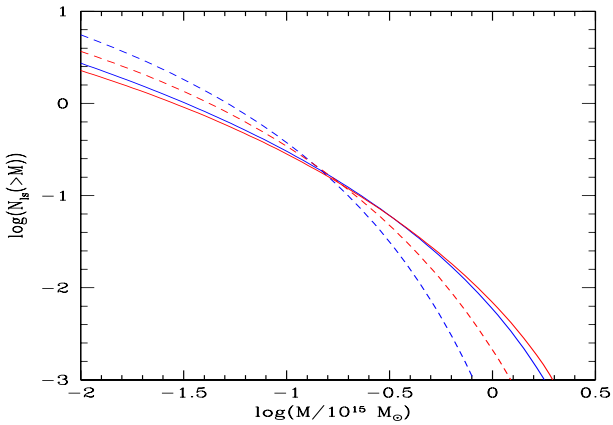

Fig. 3. The mean number of clusters $\mathcal{N}_{ls}(> M)$ of mass larger than M which intersect a line of sight between $z = 0$ and $z = 2$ (the contribution of higher redshifts is negligible). The solid lines correspond to the scaling prescription and the dashed lines to the PS approach, for both SCDM and OCDM scenarios. In both cases the number of very massive clusters is larger for the open universe.

$$\frac{d\mathcal{N}}{dz}(> 5\times 10^{14} M_\odot) = \left(\frac{\pi}{180}\right)^2 \frac{dV}{d\Omega dz} \int_{5\times 10^{14} M_\odot}^{\infty} \eta(M) \frac{dM}{M} \quad (7)$$

where $dV/d\Omega dz$ is the comoving volume element per unit steradian and unit redshift. The normalization of the PS prediction is lower than for the scaling approach as explained above (we count halos which are in the tail of the mass function). The main result of this figure is to emphasize the difference between the two cosmologies of the redshift evolution. Thus, for $\Omega_{\rm m} = 1$ the number of such clusters reaches a maximum at $z \sim 0.3$, while for $\Omega_{\rm m} = 0.3$ the peak corresponds to $z \sim 0.45$ and the evolution is slower.

2.3. Counts along the line of sight

From the cluster multiplicity function we can derive the mean number of clusters $\mathcal{N}_{ls}(> M, < z)$ of mass larger than M which intersect a line of sight between $z = 0$ and a given redshift z:

$$\mathcal{N}_{ls}(> M, < z) = \int_0^z c\frac{dt}{dz}(1+z)^3 dz \int_M^\infty \frac{dM}{M} \eta(M) \pi R^2.$$

The result is displayed in Fig. 3. Of course, we recover the difference between the scaling model and the PS approach we described above for the mass functions. The open universe gives higher counts for very massive halos because of the slower decline with redshift of the mass function. Note however that for the scaling prescription the difference between the two cosmologies is quite small. Of course this would change with another choice for σ_8. We see that the mean number of clusters on a line-of-sight is quite small since we typically have $\mathcal{N}_{ls} < 1$.

3. Cluster temperature function

Although the study of cluster mass functions is convenient from a theoretical point of view, for observational purposes it is more interesting to consider temperature functions. For this we need the temperature which is associated with halos of a given mass.

3.1. Characteristic temperature of the halos

The Jeans equation for the velocity dispersion σ_v of the dark matter yields:

$$\frac{d}{dr}(\rho\sigma_v^2) = -\rho\,\frac{\mathcal{G}M(< r)}{r^2}. \quad (8)$$

In the case of an isothermal density profile $\rho(r) \propto r^{-2}$ this leads to:

$$\sigma_v^2(R) = \frac{\mathcal{G}M}{2R} \quad \text{and} \quad kT = \frac{\mathcal{G}\mu m_p M}{2R}, \quad (9)$$

where we defined the virial temperature T of the halo by $kT = \mu m_p \sigma_v^2$ and R is the virial radius of the cluster. Here μm_p is the mean molecular weight of the gas and m_p is the proton mass. For a different density profile we would still obtain (9) for the mean temperature, with a multiplicative factor of order unity. We assume that the mass of baryons M_b is proportional to the mass of the dark matter halo M:

$$M_b = \frac{\Omega_{\rm b}}{\Omega_{\rm m}}\, M, \quad (10)$$

where $\Omega_{\rm b}$ is the present ratio of the baryon density to the critical density. With these parameters, using the fact that halos are defined by the density contrast $\Delta_c(z)$, we have:

$$M \propto \Omega_{\rm m}(1+\Delta_c)(1+z)^3 R^3 \quad (11)$$

where R is the virial radius of the cluster, and Eq. (9) writes:

$$T = T_0\ M_{15}^{2/3}\ \Delta_c(z)^{1/3}\ (1+z) \quad (12)$$

with

$$M_{15} = \left(\frac{M}{10^{15}\ M_\odot}\right) \quad \text{and} \quad T_0 = 1.2\ \Omega_{\rm m}^{1/3}\ h^{2/3}\ \text{keV}.$$

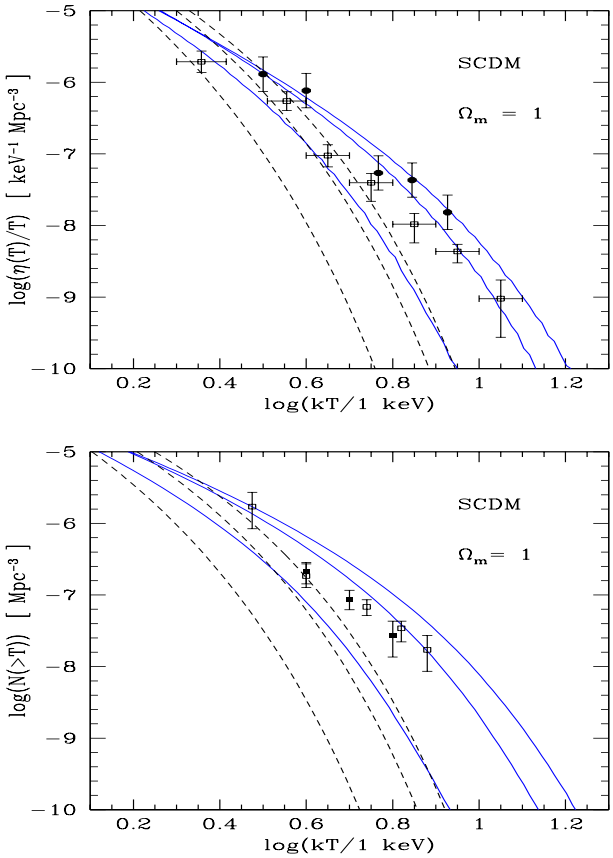

Fig. 4. *Upper panel*: the comoving cluster X-ray temperature function $\eta(T)\ dT/T$ for the SCDM scenario. The solid lines correspond to the scaling prescription while the dashed lines represent the PS formulation. We display the redshifts $z = 0.05$, $z = 0.33$ and $z = 1$ (a larger z corresponds to fewer bright clusters). The data points are observational results at $z = 0$ from Henry & Arnaud (1991) (disks) and Edge et al. (1990) (squares). *Lower panel*: the cumulative cluster temperature function at the same redshifts. The open and filled squares are observations from Henry (1997) at $z = 0.05$ and $z = 0.33$ respectively.

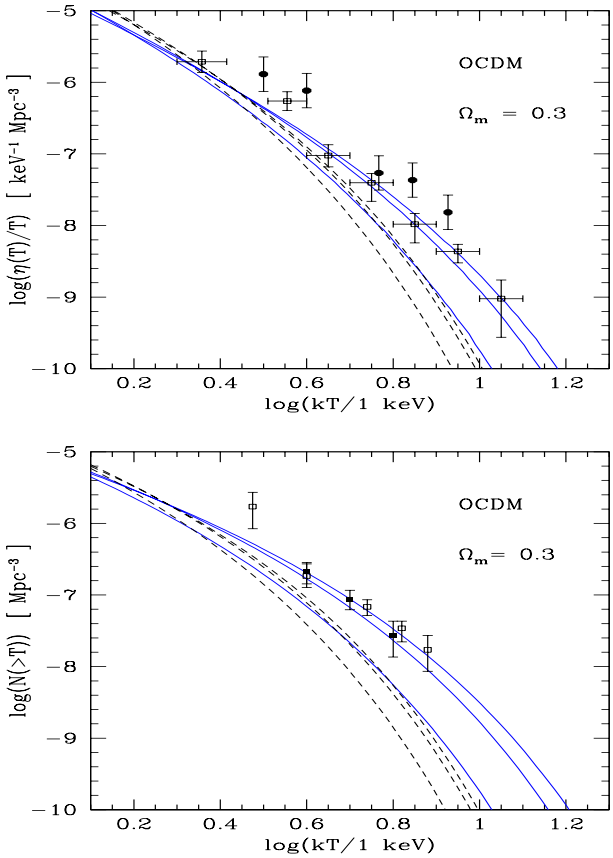

Fig. 5. The comoving differential and cumulative temperature functions as in Fig. 4, for the case of an open universe with $\Omega_{\rm m} = 0.3$.

This is consistent with numerical simulations which recover this scaling law, with a similar normalization. In these units, Navarro et al. (1995) find $T_0 = 1.4\ \Omega_{\rm m}^{1/3}\ h^{2/3}$ keV while Evrard et al. (1996) get $T_0 = 1.2\ \Omega_{\rm m}^{1/3}\ h^{2/3}$ keV.

3.2. Evolution with redshift of the temperature function

Using $\eta(T)dT/T = \eta(M)dM/M$ we can get the cluster temperature function from (12) and (5) or (2). Its evolution with redshift is shown in Fig. 4 and Fig. 5. Note that the temperature T we consider in this section is the virial temperature. Indeed, for the hot clusters ($T \gtrsim 1$ keV) we study here it is also the temperature of the gas which is heated by shocks during the gravitational collapse. In contrast, in cool groups ($T \lesssim 1$ keV) the gas is also influenced by a possible preheating of the IGM (e.g., Valageas & Silk 1999b) which leads to a smoother baryonic density profile and a larger gas temperature. This is discussed in Sect. 5.

First, we can check that the difference between the scaling prescription and the PS prediction is similar to the trend we obtained for the mass functions in Sect. 2.2. In particular, we can note that Governato et al. (1999) found that for a standard SCDM model ($\Omega_{\rm m} = 1$) normalized to $\sigma_8 = 0.5$ (which is our case) the PS prescription underestimates the number of hot clusters $kT > 7$ keV by almost a factor 10 at $z = 1$, while it overestimates the number of small halos. These authors also found that the deficiency of massive halos predicted by the PS approach gets more severe for smaller σ_8 (hence also at higher redshifts). In our view (see the discussion in VS), this is simply due to the fact that in this case one looks at rarer objects, farther in the cutoff of the mass function, which increases the discrepancy between both theoretical mass functions which have different exponential tails. However, the discrepancy between the PS and the scaling predictions is again slightly larger than what these numerical results imply at the large mass end.

Next, we can check that the redshift evolution of the temperature function is faster for the critical density universe than for the open case, in agreement with Fig. 1 for the mass function (see also Oukbir & Blanchard 1997). Thus, the very small decline with z of the observed cluster temperature function (Henry 1997) from $z = 0.05$ to $z = 0.33$ favors the open case (or more generally a low-density universe). However, the redshift evolution of the cluster temperature function we obtain in the SCDM

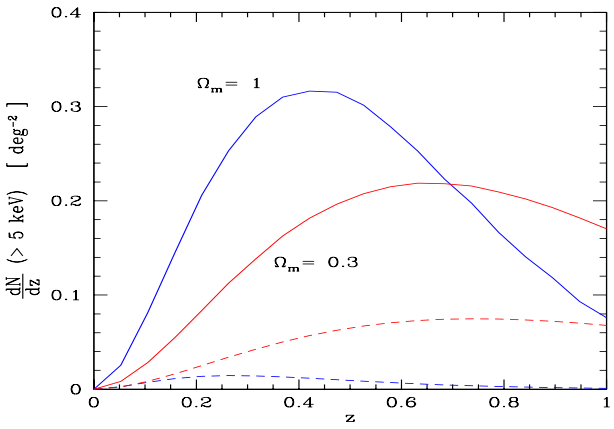

Fig. 6. The redshift distribution per square degree of clusters hotter than 5 keV, for $\Omega_{\rm m} = 1$ and $\Omega_{\rm m} = 0.3,\ \Omega_\Lambda = 0$, with a CDM power-spectrum. The graph shows the number of clusters $d\mathcal{N}/dz(> 5\,{\rm keV})$ per unit redshift interval and square degree. The solid lines correspond to the non-linear prescription while the dashed lines represent the PS formulation. The open universe corresponds to the slowest redshift evolution.

case, is not much faster than the observed decline and our study shows it cannot be ruled out. Note that we could obtain a better agreement with the data for $\Omega_{\rm m} = 1$ by choosing a slightly lower σ_8. However, the normalization of the power-spectrum we use is constrained by our previous studies of galaxies, quasars and Lyman-α clouds since we want to build a unified consistent model. Hence we must choose a value which provides good results for all these objects. Moreover, as explained in Sect. 2 massive clusters correspond to mildly non-linear scales close to the theoretical limit of validity of the scaling model, so that we may slightly overestimate the number of very massive clusters. Thus the value $\sigma_8 = 0.5$ used for $\Omega_{\rm m} = 1$ (which is also the result obtained by Governato et al. 1999) seems satisfactory.

The redshift evolution of the temperature function is slower than the change in the mass function which was presented in Fig. 1. This is due to the temperature-mass relation (12) which implies that $T \propto M^{2/3}\ \Delta_c(z)^{1/3}\ (1+z)$. Thus, the temperature which corresponds to a given mass increases with z, which enhances the redshift evolution of the mass function as compared with the temperature function.

The redshift distribution of clusters hotter than 5 keV, per square degree, is shown in Fig. 6. Of course, our results are similar to Fig. 2.

4. Sunyaev-Zel'dovich effect

An indirect method to get observational constraints on the cluster temperature function is to measure the Sunyaev-Zel'dovich (SZ) effect (Sunyaev & Zel'dovich 1972) due to the hot gas in the intra-cluster medium. As compared to the X-ray luminosity function which we discuss below in Sect. 5, the SZ effect presents two strong advantages: it does not depend on the detailed density profile of the gas distribution within clusters and it is more sensitive to high-redshift objects. Hence in this section we describe our predictions for this indirect measure of the cluster multiplicity function.

First, we recall that the variation of the CMB brightness at the frequency ν along the line-of-sight due to the SZ effect can be written as (e.g., Barbosa et al. 1996):

$$i_\nu = y\ j_\nu(u), \tag{13}$$

where j_ν describes the spectral form of the distortion, independent of the cluster, and y is the Compton parameter given by an integration along the line-of-sight through the cluster:

$$y = \int n_e \sigma_T \frac{kT_g}{m_e c^2} dl. \tag{14}$$

Here, T_g is the temperature of the electrons in the intracluster gas (which we approximate by the virial temperature T), m_e the electron mass, n_e the electron number density and $\sigma_T = 6.65\ 10^{-25}$ cm^2 the Thompson cross section. Defining the dimensionless frequency $u = h_p\nu/kT_0 = \lambda_0/\lambda$ where h_p is Planck constant and $\lambda_0 = 5.28$ mm for $T_0 = 2.726$ K, T_0 being the present temperature of the CMB, one can write:

$$j_\nu(u) = 2\frac{(kT_0)^3}{(h_p c)^2}\frac{u^4 e^u}{(e^u-1)^2}\left(\frac{u}{\tanh(u/2)} - 4\right). \tag{15}$$

The flux $S_\nu(u)$ of the cluster, in mJy $= 10^{-26}$ erg s^{-1}cm^{-2}Hz^{-1}, is simply the integral of i_ν over the solid angle subtended by the cluster:

$$S_\nu(u) = j_\nu(u)\ r_d(z)^{-2} \int n_e \sigma_T \frac{kT_g}{m_e c^2} dV \tag{16}$$

where:

$$r_d(z) = \frac{2c}{H_0 \Omega_{\rm m}^2 (1+z)^2} \times \left[\Omega_{\rm m} z + (\Omega_{\rm m} - 2)\left(\sqrt{1+\Omega_{\rm m} z} - 1\right)\right]$$

is the angular distance of the cluster, located at redshift z. Hence, the total flux observed from an unresolved cluster depends only on the mass of gas at the temperature T_g, and not on the density profile. Moreover, we can see that y only depends on the physical properties of the cluster, and not on its redshift. Hence it is very sensitive to the cluster populations at high redshifts, which contribute in the same manner as close clusters, which means it is a useful tool to study the distant universe. Finally, in the long wavelength regime ($u \to 0$) the negative fluctuation of the CMB spectrum is simply given by:

$$\frac{\Delta T}{T} = -2y. \tag{17}$$

The total mean Compton parameter $\langle y \rangle$, averaged over all lines of sight, which only depends on the temperature distribution of the gas, can be obtained from (14):

$$\langle y \rangle = \int c dt \int \sigma_T \frac{kT_g}{m_e c^2} \frac{d\overline{n}_e}{dT_g} dT_g \tag{18}$$

where $\overline{n}_e$ is the mean electron number density. Whence:

$$\langle y\rangle = \int_0^\infty dz \frac{dt}{dz} c\sigma_T (1+z)^3 \times \int_{M_i}^\infty \frac{dM}{M}\eta(M)\frac{\Omega_{\rm b}}{\Omega_{\rm m}}\frac{M}{\mu_1 m_p}\frac{kT_g}{m_e c^2}. \quad (19)$$

The factor $(1+z)^3$ transforms the comoving mass function $\eta(M)$ we have used so far, into the mass function in proper coordinates. The cutoff at $M_i(z)$ (defined by $t_{cool} < t_H$) is due to the fact that in small halos the gas cools in less than one Hubble time t_H. The mass $M_i(z)$ we get is typically of the order of $10^{12}\ M_\odot$.

An alternative way to get $\langle y\rangle$ is to divide the line-of-sight into small length elements Δl_i, so that:

$$\langle y\rangle = \left\langle \sum_i \hat{y}_i \right\rangle \quad \text{and} \quad \langle y^2\rangle = \left\langle \left(\sum_i \hat{y}_i\right)^2 \right\rangle \quad (20)$$

where $\hat{y}_i$ is the Compton distortion due to the line element Δl_i in one random realization. In this way, we recover the previous formula (19) for $\langle y\rangle$ and we get the fluctuations of y:

$$\langle \delta y^2\rangle = \langle (y-\langle y\rangle)^2\rangle \quad (21)$$

with:

$$\langle \delta y^2\rangle = \int_0^\infty dz \frac{dt}{dz} c\sigma_T (1+z)^3 \times \left\{ \int_{M_i}^\infty \frac{dM}{M}\eta(M)\frac{\sigma_T}{\pi R^2}\left(\frac{\Omega_{\rm b}}{\Omega_{\rm m}}\frac{M}{\mu_1 m_p}\frac{kT_g}{m_e c^2}\right)^2 + \sigma_T \xi_{cc}(R_{cl},z) R_{cl}(z)(1+z)^3 \times \left[\int_{M_i}^\infty \frac{dM}{M}\eta(M)\frac{\Omega_{\rm b}}{\Omega_{\rm m}}\frac{M}{\mu_1 m_p}\frac{kT_g}{m_e c^2}\right]^2 \right\} \quad (22)$$

The first term is due to the Poisson fluctuations of the number and the mass of clusters in each line element while the second term arises from the correlations $\xi_{cc}(r,z)$ among clusters, and $R_{cl}(z)$ is the typical radius of clusters. The first term scales as the number density n_{cl} of clusters while the second term scales as $n_{cl}(\xi_{cc}(R) n_{cl} R_{cl}^3)$. Thus, the Poisson fluc tuations are greater since the number density of clusters is small ($\xi_{cc}(R) n_{cl} R_{cl}^3 \ll 1$). We show in Fig. 7 the mean Compton parameter $\langle y\rangle$ and its fluctuations $\langle \delta y^2\rangle^{1/2}$ on a line-of-sight from $z=0$ up to the redshift z. The Compton parameter $\langle y\rangle$ is larger for the open universe because the cluster mass function declines more slowly at higher z and the line-element is slightly larger. Since the number of clusters on the line-of-sight is rather small (see Fig. 3) the fluctuations of y are of the same magnitude as the mean $\langle y\rangle$. Of course $\langle \delta y^2\rangle^{1/2}$ is much larger than $\langle y\rangle$ for $z \simeq 0$ since the number of clusters tends to 0 in this limit. In particular, at $z \simeq 0$ we have:

$$\langle y\rangle \propto \left[(1+z)^{3/2} - 1\right] \quad \text{and} \quad \langle \delta y^2\rangle^{1/2} \propto \langle y\rangle^{1/2}. \quad (23)$$

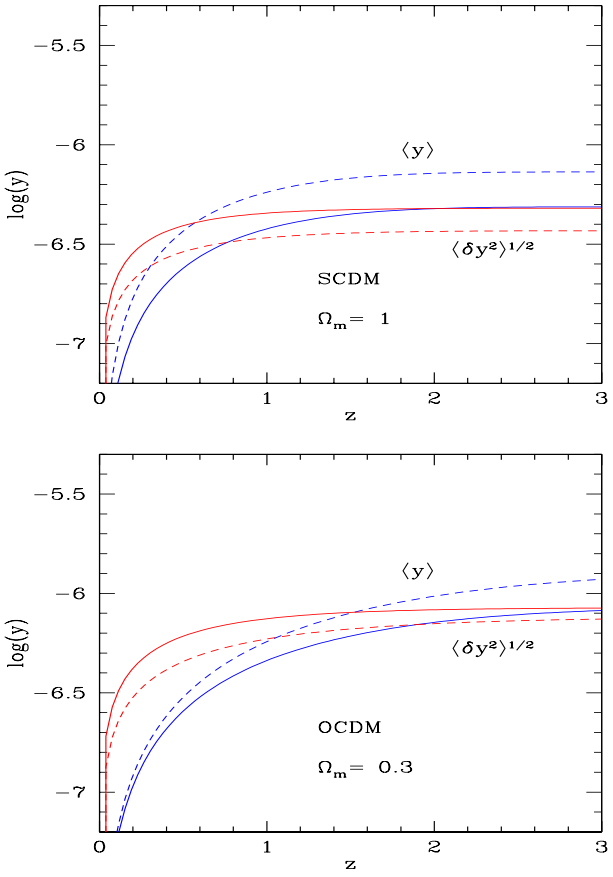

Fig. 7. *Upper panel*: the Compton parameter y, and its fluctuations $\langle \delta y^2\rangle^{1/2}$, on a line-of-sight from $z=0$ up to the redshift z, for the case $\Omega_{\rm m}=1$. The solid lines correspond to the scaling formulation and the dashed lines to the PS prescription. In both cases the fluctuation $\langle \delta y^2\rangle^{1/2}$ is the curve which shows the steepest rise at $z=0$. *Lower panel*: same curves for an open universe with $\Omega_{\rm m}=0.3$.

Note that the COBE/FIRAS upper limit is $\langle y\rangle < 1.5\times 10^{-5}$ (Fixsen et al. 1996). Thus, in both cosmologies the Sunyaev-Zel'dovich effect as measured by y is still one order of magnitude below the upper limit provided by present observations. Such a distorsion, however, will be within the reach of the MAP and PLANCK projects.

From the cluster mass function we can derive the flux density distribution of clusters $\eta(S_\nu) dS_\nu/S_\nu$. Hence, the number of SZ sources per unit solid angle on the sky with a total monochromatic flux greater than S_ν (we assume that the objects are unresolved) is

$$\frac{d\mathcal{N}}{d\Omega}(>S_\nu) = \int dz \frac{dV}{d\Omega dz}\int_{M_i'}^\infty \eta(M,z)\frac{dM}{M}. \quad (24)$$

The cutoff $M_i'(S_\nu,z)$ corresponds to the threshold S_ν. The SZ source counts at $\lambda = 0.75$ mm are shown in Fig. 8 as a function a S_ν for both cosmologies. As for the Compton parameter y, the open universe leads to slightly higher counts because of the slower decline of the cluster multiplicity function and of the larger volume element.

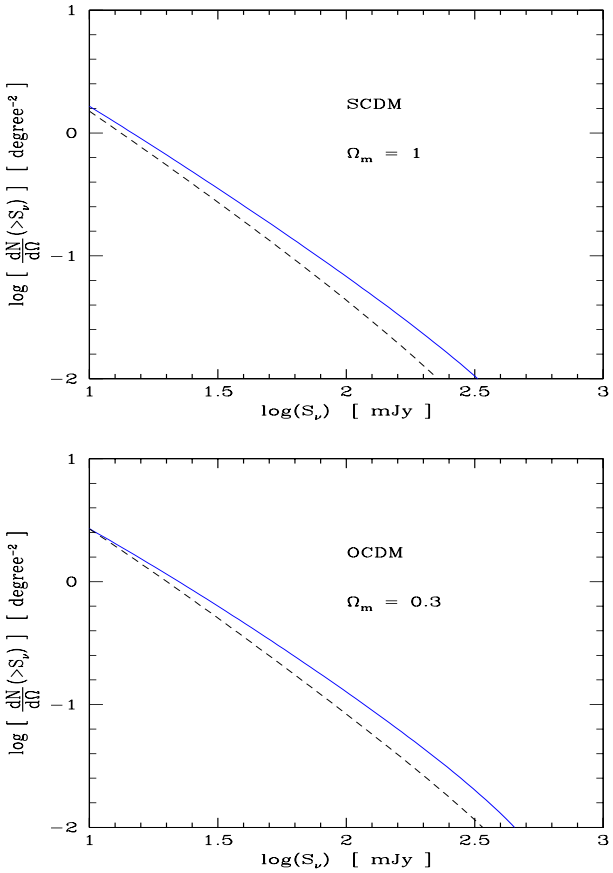

Fig. 8. *Upper panel*: the SZ source counts at $\lambda = 0.75$ mm for the SCDM case. The solid line corresponds to the scaling formulation and the dashed line to the PS prescription. *Lower panel*: same curves for an open universe.

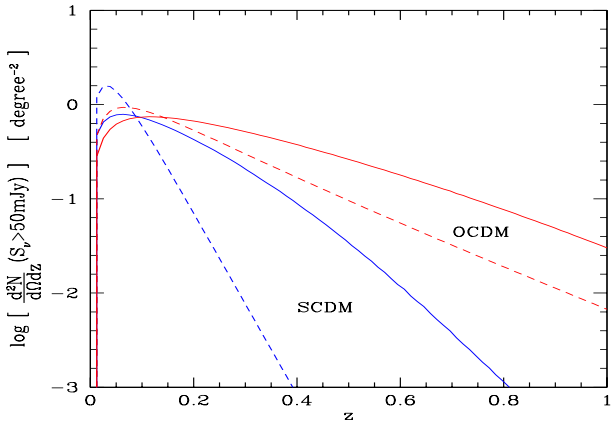

Fig. 9. The redshift distribution of SZ source counts for the SCDM and OCDM scenarios at $\lambda = 0.75$ mm. The solid lines are the scaling formulation and the dashed lines the PS prescription. The low-density cosmology corresponds to the slowest decline at large z of the SZ counts.

The redshift distribution of these source counts is displayed in Fig. 9. Of course, as explained above, the open universe predicts a slower decline at large z of the source counts than for a SCDM scenario.

5. Evolution of the X-ray luminosity function

Although observations can provide an estimate of the cluster temperature function they can more easily give the X-ray luminosity function, since it is easier to measure the luminosity of a distant cluster than its temperature. Hence we describe in this section a model to obtain the X-ray luminosity of clusters of galaxies. Moreover, the temperature-luminosity relation also contains some interesting information on a possible reheating of the IGM.

5.1. The temperature-luminosity relation

5.1.1. Breaking the simple scale-invariance

The bolometric X-ray luminosity L_{bol} of a cluster of volume V is

$$L_{bol} = \epsilon \int_V n_e^2 \Lambda_b(T_g) dV \qquad (25)$$

where ϵ is a constant of order unity, n_e is the electron number density and $\Lambda_b(T_g)$ is the emissivity function (in erg cm^3 s^{-1}) for a gas at the temperature T_g. Thus, contrary to the Sunyaev-Zel'dovich effect, see (16), the X-ray luminosity strongly depends on the density profile of the hot gas within the cluster. Using (12) and the fact that $\Lambda_b(T) \propto \sqrt{T}$ for bremsstrahlung one expects (Kaiser 1986):

$$L_{bol} \propto T_g^2. \qquad (26)$$

Note that this power-law behaviour is related to the scale-invariance of clusters: more massive objects are identical to smaller ones after a simple rescaling. However, observations show a much steeper slope $L_{bol} \propto T_g^{2.88}$ (Arnaud & Evrard 1999) and suggest a bend in the temperature-luminosity relation. Hence some physics is missing in the derivation leading to (26). In particular, one needs to break the scaling laws which led to (26) through the introduction of additional dimensional quantities. It has been suggested in the litterature (e.g., Evrard & Henry 1991; Cavaliere et al. 1997; Ponman et al. 1999; Lloyd-Davies et al. 2000) that one needs to take into account the reheating of the IGM, prior to cluster formation, which raises its entropy and can modify the gas dynamics in cool clusters. Indeed, if this entropy "floor" is sufficiently large, the gas is heated by the adiabatic compression up to a temperature which can be as large as the virial temperature of the halo. In this case the density profile of the gas is much smoother than the distribution of the dark matter, which diminishes the luminosity of these cool clusters and modifies the relation $T_g - L_{bol}$. Such a reheating of the IGM by quasars or supernovae was studied in Valageas & Silk (1999b) where it was shown that the energy provided by quasars may be sufficient to reheat the IGM. The energy delivered by supernovae was found by the latter authors to be rather small, but a more thorough estimate is under way. In this article, we simply assume that such processes have reheated the gas to a characteristic temperature $T_{ad} \sim 0.4\,$keV.

This breaks the simple scaling laws and can lead to a non-trivial temperature-luminosity relation.

5.1.2. Density profiles of the gas and of the dark matter

In order to obtain the distribution of the gas, we need the density profile of the dark matter, which is gravitationally dominant. Here we assume that the halos obey the density profile obtained in high-resolution simulations by Moore et al. (1999b):

$$\rho(r) = \frac{\rho_c}{(r/r_s)^{1.5}\,[1+(r/r_s)^{1.5}]} \quad \text{with} \quad r_s = \frac{R}{c} \tag{27}$$

where c is the concentration parameter. We use $c = 4$ as in Moore et al. (1999b), although this parameter may slightly depend on the mass of the cluster. Moreover, we assume hydrostatic equilibrium for the gas. We consider two models for the temperature p rofile $T_g(r)$ of the gas.

First, we write:

$$T_g(r) = T_s(r) + T_{ad}\left(\frac{\rho_g(r)}{(1+\Delta_c)\bar{\rho}_b}\right)^{\gamma_s-1} \tag{28}$$

where $\gamma_s = 5/3$. The first term on the right hand side in (28) describes non-adiabatic gravitational heating through shocks during the formation of the cluster. The second term takes into account the reheating of the gas, before the formation of the cluster, and its subsequent heating through the adiabatic compression during the infall. Note that the relation (28) assumes that the thermal conduction is small (e.g., Sarazin 1988) so that the gas is not exactly isothermal. In a fashion similar to (9) we write:

$$T_s(r) = \frac{\mathcal{G}\mu m_p M(<r)}{2kr} = T\,\frac{\ln\left(1+(r/r_s)^{1.5}\right)}{\ln\left(1+c^{1.5}\right)}\,\frac{R}{r} \tag{29}$$

which also measures the depth of the potential well. This also satisfies the Jeans Eq. (8) within a factor 2. Then, the distribution of the gas is given by the condition of hydrostatic equilibrium:

$$\frac{dP}{dr} = -\,\rho_g\,\frac{\mathcal{G}M(<r)}{r^2} \quad \text{with} \quad P = \frac{\rho_g k T_g}{\mu m_p}. \tag{30}$$

However, in practice we use a simplified model. From (30) one can check that at large radii where $T_g \simeq T_s(r)$ the gas follows the dark matter while at small radii below R_{core} where both terms in (28) are equal, the gas density saturates. Indeed, when $T_g \gg T_s$ the gas no longer falls into the potential well and a core with a nearly constant baryon density appears. This model is similar to those used in Cavaliere et al. (1997,1998) or Wu et al. (1999) except that these authors use the dark matter density profiles given by Navarro et al. (1996) and they do not take into account the first term on the right hand side in (28) (they use a polytropic equation of state). However, in all cases the behaviour of the gas distribution is the same: for smaller halos the preheating becomes more important and the gas density profile gets flatter which decreases the X-ray luminosity. Here, in order to simplify the calculations we approximate the gas distribution by the same profile (27) as for the dark matter in the outer parts $r > R_{core}$ and by a constant value in the core $r < R_{core}$:

$$\begin{cases} r > R_{core} \;:\; \rho_g(r) = \dfrac{\Omega_{\rm b}}{\Omega_{\rm m}}\,\rho(r) \\ \\ r < R_{core} \;:\; \rho_g(r) = \rho_{core} = \dfrac{\Omega_{\rm b}}{\Omega_{\rm m}}\,\dfrac{M(<R_{core})}{4\pi R_{core}^3/3} \end{cases} \tag{31}$$

which ensures that the total mass is conserved.

Second, we consider an alternative model where the temperature of the gas is given by:

$$T_g(r) = T_s(r) + T_{ad}. \tag{32}$$

As in (28) two processes govern the temperature of the gas: gravitational heating (first term) and a second unspecified source of energy (e.g., SNe or QSOs) which breaks the scaling law described in Sect. 5.1.1 (second term). However, in contrast to (28), here we take this additional term to be constant. Hence this model corresponds to a uniform "post-heating" of the gas which occurs after the formation of the cluster, for instance through the SNe which may eject some energy into the intra-cluster medium during and after the infall of the gas into the potential well of the cluster. From another point of view, this can also be seen as a specific case of the "pre-heating" model (28) with a different equation of state: $\gamma_s \simeq 1$. Then, this allows us to estimate the sensitivity of our model (28) to the assumed value for γ_s. Next, from the relation (32) we proceed exactly as from (28) to obtain the density distribution of the gas, described by a core radius R_{core} as in (31), which is now defined by $T_s(R_{core}) = T_{ad}$.

5.1.3. Cooling radius

In addition to the core described above which appears for the gas distribution, cooling may affect the distribution of hot X-ray emitting gas. Indeed, in the inner parts of the cluster the density can be large enough to lead to a small cooling time so that a cooling flow develops. Then, some of the gas forms a cold component which does not emit in X-ray any longer. Thus, we define the cooling radius R_{cool} as the shell where the cooling time t_{cool} becomes equal to the Hubble time $t_H(z)$:

$$t_{cool} = t_H \quad \text{with} \quad t_{cool} = \frac{3\mu_1^2 m_p k T_g}{2\mu\rho_g\Lambda_c(T_g)}, \tag{33}$$

where $\Lambda_c(T_g)$ is the cooling function. At large radii $r > R_{cool}$ the local cooling time is larger than the Hubble time. In this case, the gas distribution and the temperature have not had time to evolve much and the X-ray emissivity is proportional to $\rho_g^2\;\Lambda_b(T_g)$, see (25). On the other hand, within the cooling radius R_{cool} the gas has had time to cool and to form dense cold clouds. However, we consider that some of the gas is still hot and emits in X-ray as cooling does not proceed in a uniform fashion (Nulsen 1986; Teyssier et al. 1997; Waxman & Miralda-Escude 1995). Indeed, the cooling instability leads to a wide range of gas temperatures and densities as overdense regions cool faster and contract (because of the pressure of the surrounding gas) which increases even further their density contrast. Then, some

of the gas is simply removed from the X-ray emitting component as these dense cold clouds decouple from the hot phase. On the other hand, the temperature of the hot gas remains close to $T_s(r)$, introduced in (29), through adiabatic compression and possible gravitational heating, see Nulsen (1986, 1998) for detailed models of this multiphase ICM. The density of the hot component must be of order ρ_{cool}, defined by the condition $t_{cool} = t_H$, since the density has not had time to decrease further yet (note that the system is not stationary). As this multiphase medium is connected to the outer parts of the cluster $r > R_{cool}$ which also provide a reservoir of matter and energy, we assume that the hot low-density phase is spread all over the radius R_{cool}. Note that the time-scale for hydrostatic equilibrium is $t_p \sim r/c_s \sim t_{dyn}$ for gas at the temperature T_s (where c_s is the sound speed while t_{dyn} is the dynamical time). Since the time-scale of the infall of the gas cannot be smaller than t_{dyn} and is actually expected to be larger (the pressure and possible energy injection from SNe or gravitational interactions slow down the motion) there should be approximate pressure equilibrium. Hence at small radii $r < R_{cool}$ we write for the density of the X-ray emitting gas:

$$r < R_{cool} \; : \quad \rho_{gX}(r) = \rho_{cool} = \rho_g(R_{cool}) < \rho_g(r) \qquad (34)$$

while at large radii $r > R_{cool}$ we have $\rho_{gX}(r) = \rho_g(r)$. For cool clusters where the non-gravitational energy term T_{ad} plays an important role, the distribution of the gas is flatter than the dark matter and it shows a core of constant density ρ_{core}. Then, the cooling time at this core radius R_{core} is still longer than the Hubble time so that cooling plays no role: the luminosity of the cluster is determined by the radius R_{core} due to the distribution of the gas itself. On the other hand, for hot clusters the gas follows the dark matter density profile over a large range of radii and the cooling time gets smaller than the Hubble time in the "outer region" $r > R_{core}$. In this case, the distribution of the X-ray emitting gas is characterized by the cooling radius R_{cool} and the luminosity of the cluster is governed by the cooling criterium. Note that R_{cool} mainly plays the role of a cutoff for the distribution of X-ray emitting gas: we would obtain similar results for a model where we set $\rho_{gX}(r) = 0$ for $r < R_{cool}$, as most of the X-ray emission comes from the regions $r \sim R_{cool}$ (thus such a model would simply decrease the luminosity by a numerical factor ~ 2 which can be absorbed in the normalization of t_{cool} for instance).

In Valageas & Silk (1999b) we used for illustrative purposes an isothermal model for the dark matter and the gas distribution, with the relation (32) (interpreted as $\gamma_s = 1$). Thus, we had:

$$\rho(r) \propto r^{-2} \quad \text{and} \quad \rho_g(r) \propto \rho^{-\beta} \quad \text{with} \quad \beta = \frac{T}{T + T_{ad}}, \qquad (35)$$

where T is the virial temperature of the cluster defined in (9) and the gas distribution was obtained from the hydrostatic equilibrium condition (30). Here, the distribution of the gas does not show a core radius R_{core} while the X-ray emitting gas is still characterized by a cooling radius R_{cool}. However, it is easy to check that we recover a behaviour similar to the case discussed above. Indeed, for hot clusters with $T > 3T_{ad}$ the density profile of the gas is very steep ($\beta > 3/4$) so that the X-ray emissivity is dominated by the inner parts of the cluster - as can be seen from (25) and (35) - hence by the cooling radius R_{cool}. On the other hand, for cool clusters with $T < 3T_{ad}$ the density profile of the gas is rather flat ($\beta < 3/4$) which means that the luminosity of the cluster is governed by the outer parts $r \sim R$. In this paper, for cool clusters the emissivity is dominated by the regions $r \sim R_{core}$ and $R_{core} = R$ for low temperature clusters ($T \leq T_{ad}$).

Thus, we see that the main characteristics of clusters do not strongly depend on the details of the models (density profile of the dark matter halo, index γ_s of the "equation of state") as they are mainly sensitive to T_{ad}.

5.1.4. Evolution of the temperature – X-ray luminosity relation

For both models described above we obtain the X-ray luminosity from (25), where n_e is given by the density of the X-ray emitting gas ρ_{gX}. We determine the factor ϵ by requiring (25) to reproduce the observations for massive clusters ($T_g > 1\,\mathrm{keV}$). We get $\epsilon = 2.2$ (resp. $\epsilon = 0.8$) for a critical density universe (resp. an open universe). We show in Fig. 10 and in Fig. 11 the temperature-luminosity relation we obtain for both models (28) and (32), with the above value of ϵ and $T_{ad} = 0.5\,\mathrm{keV}$ (resp. 0.4 keV) for the SCDM (resp. OCDM) cosmology. The gas temperature used in the figures is $T_g = T + T_{ad}$. We can see that we get very similar results which agree reasonably well with observations. Of course, we could improve the agreement of the model (32) (i.e. $\gamma_s = 1$) with observations in the OCDM cosmology by using a slightly larger value for T_{ad}. We also note that the redshift evolution we obtain is very small, which is consistent with observations (Mushotzky & Scharf 1997). This suggests that the "preheating" temperature T_{ad} should not evolve too strongly with redshift for $z < 1$, which might favour supernovae as the source of energy (due to the sharp decline at low z of the quasar luminosity function, the characteristic temperature T_{ad} obtained within the framework of a model where the preheating is due to QSOs, is expected to show a faster evolution with z, see Valageas & Silk 1999b).

Thus, in order to recover a bend in the temperature - X-ray luminosity relation one mainly needs to introduce a new dimensional parameter, like T_{ad}, as discussed in Sect. 5.1.1. Since in this article we are only interested in the total luminosity of clusters the simple models described in Sect. 5.1.2 are sufficient for our purpose and in the following we use the model (28) (i.e. $\gamma_s = 5/3$). As shown by the comparison of Fig. 10 and Fig. 11 our predictions for the luminosity function are not very sensitive to the details of our model. We would also obtain similar results with the isothermal model (35) as in Valageas & Silk (1999b). On the other hand, this means that in order to discriminate between various models one needs precise observations of the density profiles of the gas and of the dark matter as well as a measure of the gas temperature. This will be provided by the XMM mission. However, present observations seem to favour the model (28) with a "preheating" of the gas before the formation of clusters (Lloyd-Davies et al. 2000).

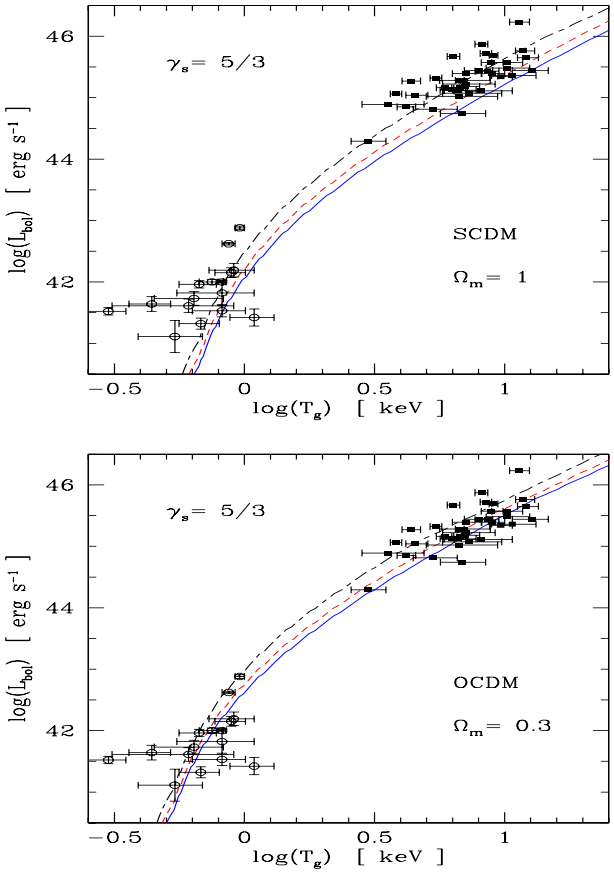

Fig. 10. The relation temperature - bolometric luminosity for clusters in the case $\gamma_s = 5/3$ for the model (28) with $T_{ad} = 0.5\,\mathrm{keV}$ (resp. $T_{ad} = 0.4\,\mathrm{keV}$) for the SCDM (resp. OCDM) scenario. The solid, dashed and dot-dashed lines correspond to $z = 0$, $z = 0.33$ and $z = 1$ respectively. The data points are from Mushotzky & Scharf (1997) ($0.14 < z < 0.55$) for clusters and from Ponman et al. (1996) ($z < 0.05$) for groups. The upper panel corresponds to a critical density universe (SCDM) and the lower panel to an open universe (OCDM).

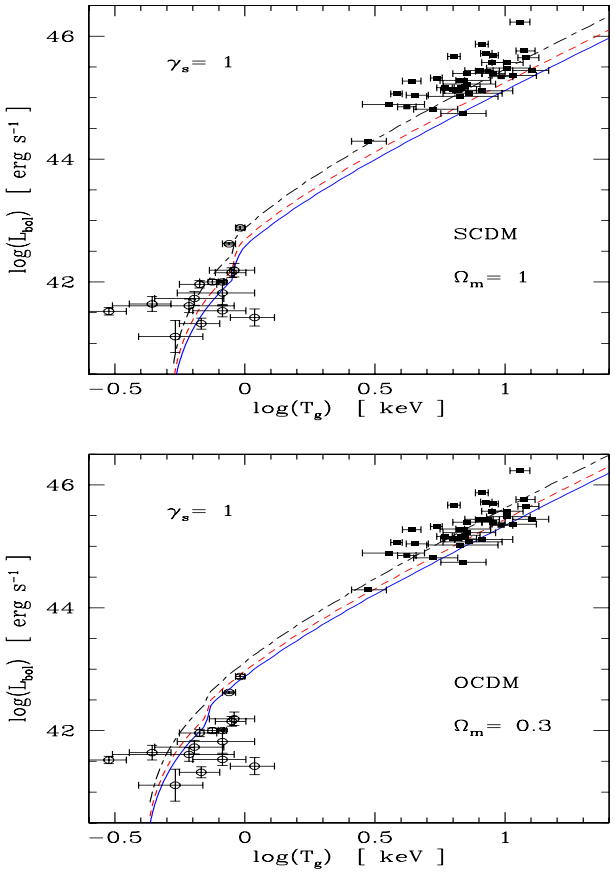

Fig. 11. The relation temperature - bolometric luminosity as in Fig. 10 for the model (32) (i.e. $\gamma_s = 1$) with the same values for T_{ad}. A larger value for T_{ad} would improve the agreement with observations at low T_g for the OCDM scenario.

5.2. Luminosity function

From the temperature-luminosity relation described in the previous section and the temperature multiplicity function obtained in Sect. 3 we can derive the cluster X-ray luminosity function. Note that the results discussed in the following are largely independent of Sect. 5.1 since any temperature-luminosity relation which agrees with observations would give similar results. From the luminosity L_{bol} obtained in the previous section we write the luminosity L_X in the frequency band $\nu_1 - \nu_2$ as:

$$L_X = L_{bol}\,\left(e^{-h_P\nu_1/kT_g} - e^{-h_P\nu_2/kT_g}\right). \qquad (36)$$

Here h_P is Planck constant and we neglected the variation of the Gaunt factor. We compare our predictions with observations in Fig. 12 for both cosmological scenarios, in the rest-frame frequency band 0.5–2 keV. First, we note that we recover the fact that the scaling model predicts more massive and bright clusters but fewer small and faint objects than the PS approach. Then, we see that for the critical density universe, the luminosity function we obtain predicts too many faint clusters. This could be cured by a small change of the initial power-spectrum. Of course, in a similar fashion one can also bring the PS prescription in agreement with observations. However, we prefer to keep this normalization of the power-spectrum in order to be consistent with our previous articles about galaxies and Lyman-α clouds and with results from numerical simulations (Governato et al. 1999). On the other hand, for the open universe our predictions agree reasonably well with the data. We can see that for both cosmological scenarios the redshift evolution we get is very small, which is consistent with observations.

We display in Fig. 13 the integrated cluster surface density above an X-ray flux threshold S_X in the frequency band 0.5–2 keV:

$$\frac{d\mathcal{N}}{d\Omega}(>S_X) = \int dz \frac{dV}{d\Omega dz} \int_{M_i'}^{\infty} \eta(M,z)\frac{dM}{M}. \qquad (37)$$

The cutoff $M_i'(S_X, z)$ corresponds to the X-ray flux S_X. It is obtained from the temperature-luminosity relation and the flux-luminosity relation:

$$S_X = \frac{L_X}{4\pi r_{lum}(z)^2}, \qquad (38)$$

where the distance $r_{lum}(z)$ is the luminosity distance up to redshift z. Here the luminosity L_X is obtained as in (36) with

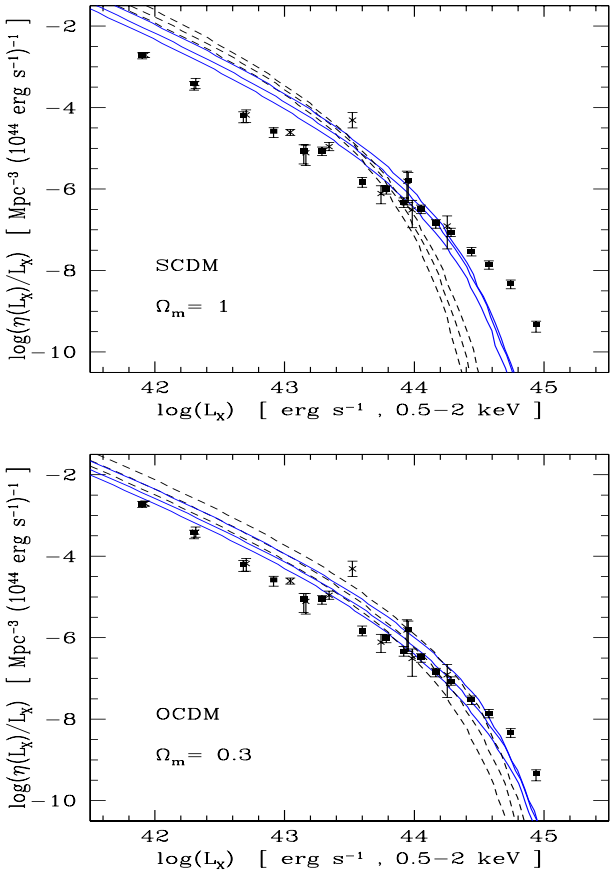

Fig. 12. The comoving cluster luminosity function in the rest-frame 0.5–2 keV band, at redshifts $z = 0$, $z = 0.33$ and $z = 1$ (smaller z corresponds to fewer faint objects). The solid lines show the scaling formulation and the dashed lines the PS prescription. The data points at $z = 0$ are from Ebeling et al. (1997) (filled squares) and Burns (1996) (crosses). The upper panel corresponds to the SCDM scenario and the lower panel to the open universe.

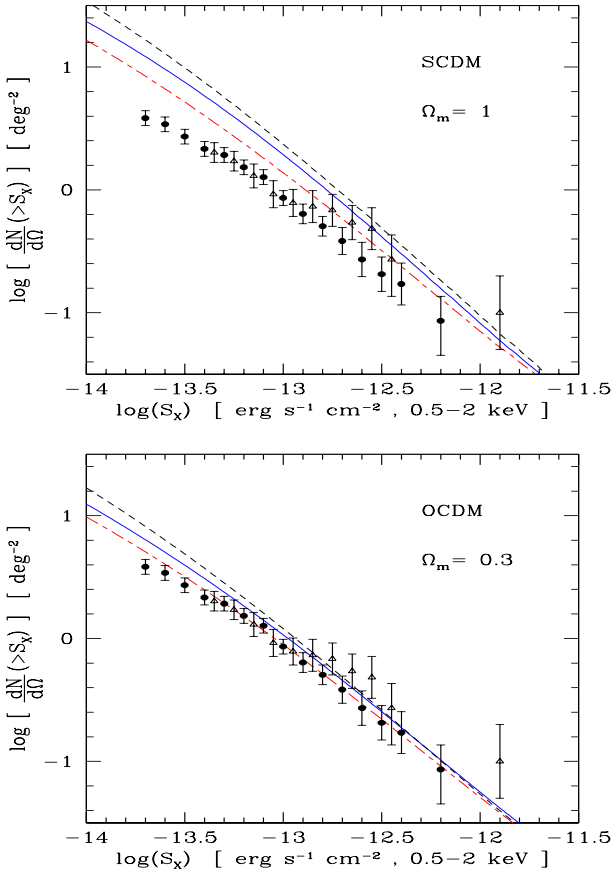

Fig. 13. The number of clusters per square degree brighter than an X-ray flux limit S_X. The solid line corresponds to the scaling formulation and the dashed lines to the PS prescription. The low dot-dashed curve is a no-evolution model. The data points are from Jones et al. (1998) (triangles) and Rosati et al. (1998) (disks). The upper (resp. lower) panel corresponds to the SCDM (resp. OCDM) scenario.

$\nu_i(z) = \nu_i(1 + z)$ to take into account the redshift of the observed frequency band 0.5–2 keV. Our results agree with observations, although our normalization is slightly too high for the critical density universe. In both panels, the dot-dashed curve corresponds to a no-evolution model where the comoving cluster luminosity function does not vary with z and remains equal to its value at $z = 0$, shown in Fig. 12. Note that evolution effects are not very large. The scaling and PS approaches give very close results, although we can still recognize that the PS approximation predicts fewer massive objects but more small halos. Indeed, this difference is somewhat smeared out in Fig. 13 because the X-ray sources seen with a given flux S_X correspond to a large variety of objects located at different redshifts.

6. Galaxies and quasars versus groups and clusters

6.1. Galaxy X-ray luminosity function

In addition to clusters, galaxies may also emit in X-rays when they form. Indeed, in order to make stars and build a galaxy the gas embedded within a dark matter halo must cool and fall into the gravitational potential well. During this process, the gas can radiate some energy in the X-ray band by bremsstrahlung, especially for the most massive galaxies with a large virial temperature $T \sim 10^7$ K ~ 1 keV. As a consequence, some of the X-ray sources one could observe on the sky may be high-redshift newly-born galaxies. Note that there will be obvious observational difficulties to distinguish X-ray emitting galaxies from small groups of similar mass, containing a few smaller galaxies.

To derive this galaxy X-ray luminosity function that is to be compared to the one for groups and rich clusters, we first need the galaxy multiplicity function.

6.1.1. Galaxy multiplicity function

We use the galaxy formation model described in detail in Valageas & Schaeffer (1999). This previous study is consistent with the present work (all parameters have the same values) and it was checked against observations for various galaxy properties. In particular, it is based on the same formalism described in Sect. 2.1 to derive the mass functions of dark matter halos.

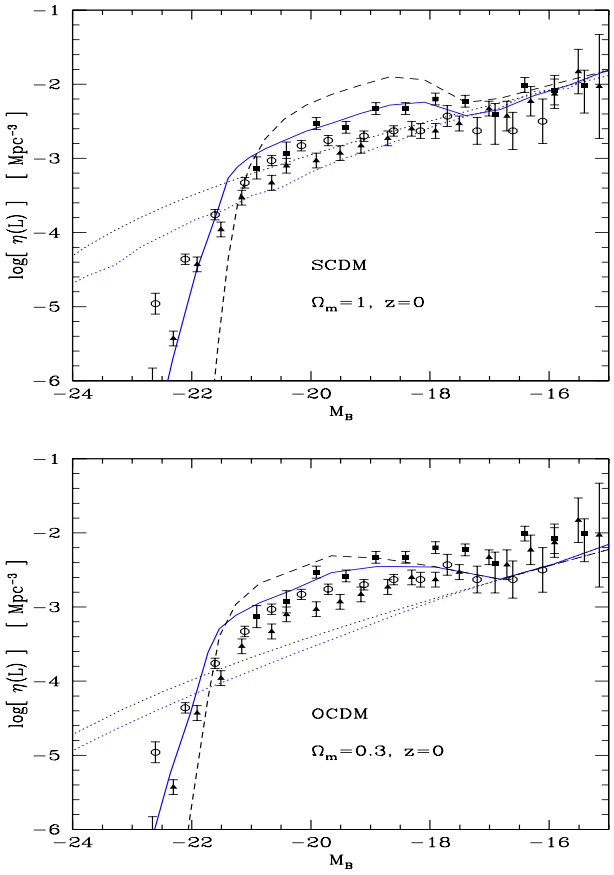

Fig. 14. The comoving galaxy B-band luminosity function at $z = 0$. The solid lines show our scaling approach and the dashed-lines a modified PS prescription. The dotted lines correspond to the scenario (C) where galaxies are defined by a constant density threshold $\Delta_c(z)$, for both prescriptions (thus the upper dotted curve is the standard PS mass function). The data points are observations from Loveday et al. (1992) (circles), Ellis et al.(1996) (filled squares) and Zucca et al. (1997) (triangles). The upper (resp. lower) panel corresponds to the SCDM (resp. OCDM) cosmology.

We briefly recall here the characteristics of this model we need for our purposes. We define galaxies by the requirement that two constraints be satisfied by the underlying dark matter halo: i) *a virialization condition* $\Delta > \Delta_c$ and ii) *a cooling constraint* $t_{cool} < t_H(z_{form})$ which states that the gas must have been able to cool within a few Hubble times at formation. We assume that the Hubble time at formation is given by the dynamical time, i.e. that the density of these dark matter halos does not evolve much after collapse. Note that just-collapsed halos ($\Delta = \Delta_c$) satisfy $t_{dyn} \sim t_H$ by definition. Thus, the dark matter radius of the halos we identify with galaxies is given by the conditions:

$$t_{cool} < t_{dyn} \qquad \text{and} \qquad \rho > (1+\Delta_c)\overline{\rho}. \tag{39}$$

In other words, the radius $R(T,z)$ of galaxies of virial temperature T at redshift z is:

$$R(T,z) = \text{Min}\,(R_{cool}, R_{vir}) \tag{40}$$

where R_{cool} is a "cooling radius" defined by $t_{cool} = t_{dyn}$ while R_{vir} is the "virial radius" defined by $\Delta = \Delta_c$. Note that for clusters, by definition, we have $R = R_{vir}$. At low redshift, for small masses, cooling is very efficient so that the virialization condition is the most constraining one in (39). Hence $R = R_{vir}$ and these galactic halos are defined by the usual density contrast threshold $\Delta_c(z)$. On the other hand, for large masses (i.e. high T) cooling is inefficient and only occursfor high gas densities, so that galactic halos are defined by $R = R_{cool}$. This means that their mean density contrast is larger than Δ_c and that these objects formed at a larger redshift than the one we would have obtained by considering just-collapsed objects defined by $\Delta = \Delta_c$. At large T, where bremsstrahlung is the main cooling process, the cooling radius goes over to a constant $R_{cool} \sim 100$ kpc. Finally, we use a simple star formation model which takes into account infall into the inner parts of the galaxy, feedback from supernovae (proportional to $1/T$ for small galaxies as in Kauffmann et al. 1993) and with a star formation time-scale proportional to the dynamical time (see Valageas & Schaeffer 1999 for details).

We recall in Fig. 14 the B-band luminosity function we obtain at $z = 0$. We can check that our predictions agree reasonably well with observations. Moreover, we can check that the "extended PS" prescription (dashed lines) predicts more intermediate mass halos and fewer very massive objects than the scaling mass function, as noted in Sect. 2.1. This is consistent with the behaviour we already found for clusters in Sect. 2.2. In addition, in order to clearly show the importance of correctly identifying the galactic halos we also display in Fig. 14 the luminosity functions we would obtain (dotted curves) for a "model" (C) where all halos are defined by the virialization constraint (constant density contrast):

$$\text{(C)}: \ \Delta_{gal}(x) = \Delta_c(z) \qquad \text{for all} \quad x \tag{41}$$

with all other parameters (i.e. the star formation model) kept unchanged. Of course, this "model" is only shown for illustrative purposes since it is clearly inadequate for massive halos. Indeed, in the case (C) at large masses we identify clusters or groups and not galaxies! Thus, we can see in Fig. 14 that for faint luminosities which correspond to small halos, the "model" (C) superposes onto our actual galaxy model while for large luminosities it leads to huge galaxies which are not observed. In particular, it implies a bright magnitude tail of the luminosity function which is much too flat. Note that Monaco et al. (2000), using a model for quasars similar to ours (see below Sect. 6.2.1), also manage to recover observations for both galaxy and quasar luminosity functions. However, in a standard procedure that has been used (Schaeffer & Silk, 1988) as soon as the PS prescription became popular, in order to correct the PS mass function so as to use it for galactic halos they multiply the PS prediction by a factor $\exp[-(M/M_{cool})^{4/3}]$ which is fitted to the cut-off of the observed galaxy luminosity function. Although this procedure can improve the mass functions it does not really deal with the "subclustering problem" itself (each massive halo still corresponds to a cluster). In contrast, our prescription has the serious advantage of taking into account this "subclustering problem" in a very natural fashion using physical arguments based on cooling conditions, (see (39)), and to count the in-

dividual galactic halos themselves so that one can study their internal properties. Moreover, it is interesting to note that in addition to a strong cutoff of the luminosity function the use of the proper constraints (39) leads to a non-trivial "plateau" in the range $-21 \lesssim M_B \lesssim -16$ which provides good agreement with observations.

6.1.2. Galaxy X-ray emission

As explained above galaxies are defined by the two constraints (39). Hence at any redshift there is a characteristic virial temperature $T_f(z)$ which marks the transition between the low temperature regime, where $R = R_{vir}$, and the high temperature regime, where $R = R_{cool}$. It increases with z and at $z = 0$ we have $T_f \sim 10^6$ K. In this approach, large objects defined by $\Delta = \Delta_c$ with a virial temperature $T > T_f(z)$ are made of several galaxies and correspond to groups or clusters. They can be subdivided into several subunits which verify the constraints (39). Of course, halos with a virial temperature which is only slightly higher than $T_f(z)$, merely consist of one galaxy with some gas falling from its surroundings which have not cooled yet. However, we shall identity just-collapsed halos above $T_f(z)$ as groups or clusters, which should provide a reasonable estimate of the transition, while we shall call just-collapsed halos below $T_f(z)$, galaxies. In particular, the mass functions of groups and clusters we used above were set to 0 for $T < T_f(z)$ (this also corresponds to the cutoff $M_i(z)$ which appeared in (19) to obtain $\langle y \rangle$). However, this has no effect on the quantities we have studied so far because we considered high virial temperatures $T > 0.5\,\mathrm{keV}$ at low redshifts $z < 1$. Since in our model galaxies below and above T_f have a rather different history we consider each regime separately.

First, we write the galaxy luminosity (due to the cooling of the gas) as:

$$L_{bol} = \frac{E}{t_{cool}} = \frac{3}{2}\frac{M_{hot}kT}{\mu m_p t_{cool}} \tag{42}$$

where M_{hot} is the mass of hot gas (i.e. of the order of the virial temperature T) and t_{cool} is its cooling time. Galaxies with $T < T_f(z)$ are defined as "just-collapsed" objects ($\Delta = \Delta_c$) and they satisfy $t_{cool} < t_H(z)$. Although the latter, by definition, have undergone a major merging event in their recent past (at a redshift $z + \delta z$ with $\delta z/(1+z) \ll 1$), all of them are not necessarily in the midst of such a process. The time which has elapsed since the last merging, is measured by t_H, so we write for the galaxy X-ray luminosity function

$$T < T_f : \quad \eta(L_{bol})\frac{dL_{bol}}{L_{bol}} = \frac{t_{cool}}{t_H}\,\eta(M)\frac{dM}{M}. \tag{43}$$

This ensures that we only count the galaxies where the gas has not had time to cool significantly since the last major merging event (while we neglect the contribution of the small objects which had time to cool). Then, the mass M_{hot} of hot gas characteristic of these objects is of the order of the total mass of gas M_g, hence we take $M_{hot} = M_g$ (and the cooling time is evaluated using the gas density $\rho_g = (1+\Delta_c)\overline{\rho}_b$). On the other hand, massive old galaxies with $T > T_f$ have already had time to cool since they satisfy $t_{cool} = t_H(z_{form}) < t_H(z)$. However, if cooling is inhomogeneous and there is an approximate pressure equilibrium, a diffuse gaseous hot component may be present in the galactic halo with a density given by the condition $t_{cool} = t_H(z)$, as we discussed in Sect. 5.1.3 for clusters. This component could be a left-over of the initial baryonic content of the galaxy (which gradually cools with time and falls into the inner parts of the galaxy to form stars) but it could also be replenished by the ejection of matter from the center of the galaxy by supernovae. In order to investigate the range of the galactic contribution to the overall X-ray emission we consider the following two models. First, we assume that there is no hot component (or it is negligible) so that in this "Cold" scenario old galaxies with $T > T_f(z)$ no longer emit in X-rays:

$$\text{(Cold)}: \quad L_{bol} = 0 \quad \text{for} \quad T > T_f(z). \tag{44}$$

This implies a sharp cutoff for the galaxy X-ray luminosity function at the luminosity which corresponds to the transition T_f (i.e. there is an upper bound for L_{bol}). Note however that these galaxies contribute to the X-ray luminosity function at the redshift z_{form}, when they formed. Second, we consider a "Hot" model where there is a diffuse hot component at the virial temperature T with a characteristic density:

$$\text{(Hot)}: \quad \rho_{hot} = \frac{3\mu_1^2 m_p kT}{2\mu\Lambda_c(T)t_H} \quad \text{for} \quad T > T_f(z). \tag{45}$$

This gives the mass M_{hot} at the galactic radius R and the luminosity L_{bol} from (42) where we now have $t_{cool} = t_H(z)$. Then, we obtain the X-ray luminosity function from the galaxy multiplicity function described in Sect. 6.1.1 as: $\eta(L_{bol})dL_{bol}/L_{bol} = \eta(M)dM/M$. In practice, we can expect the actual X-ray luminosity function in our universe to be somewhere in between these two ideal scenarios. In particular, since the cooling radius is equal to the actual radius R of the galaxy (by definition), there is not necessarily a large reservoir of hot gas at radii larger than R_{cool} to ensure that the hot phase occupies all the volume of the galactic potential well, in contrast to the case encountered for clusters. However, there may be some infall from the surrounding IGM (in addition to SNe ejecta). Hence the "Hot" scenario can be interpreted as an upper bound for the X-ray galaxy counts and the "Cold" scenario as a lower bound. Finally, we obtain the X-ray luminosity L_X in a given frequency band $\nu_1 - \nu_2$ as in (36), which allows us to derive the galaxy luminosity function in this band.

We show in Fig. 15 and Fig. 16 the galaxy X-ray luminosity functions we obtain in this way for both cosmologies in the rest-frame frequency band 0.5–$2\,\mathrm{keV}$. The solid lines (resp. dashed lines) correspond to the scaling formulation (resp. the PS prescription) for the "Hot" scenario (45). For the "Cold" model, the luminosity function vanishes at high luminosities above the cutoff $T_f(z)$ shown by the vertical solid line while it is equal to the "Hot" model prediction at fainter luminosities. As explained above the cutoff $T_f(z)$ increases with z which leads to a larger luminosity cutoff $L_f(z)$ at higher z. Below T_f the prefactor t_{cool}/t_H diminishes the contribution of small and faint

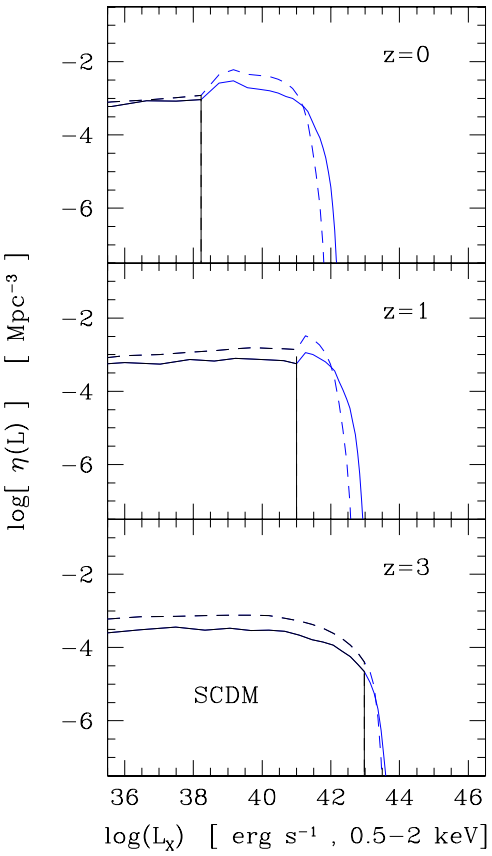

Fig. 15. The comoving galaxy X-ray luminosity function in the rest-frame frequency band 0.5–2 keV for the SCDM case. The solid line corresponds to the scaling formulation and the dashed line to the PS prescription, for the "Hot" scenario. The vertical line shows the cutoff at $T_f(z)$. For the "Cold" model the luminosity function vanishes at higher luminosities and it is equal to the "Hot" model prediction at fainter luminosities.

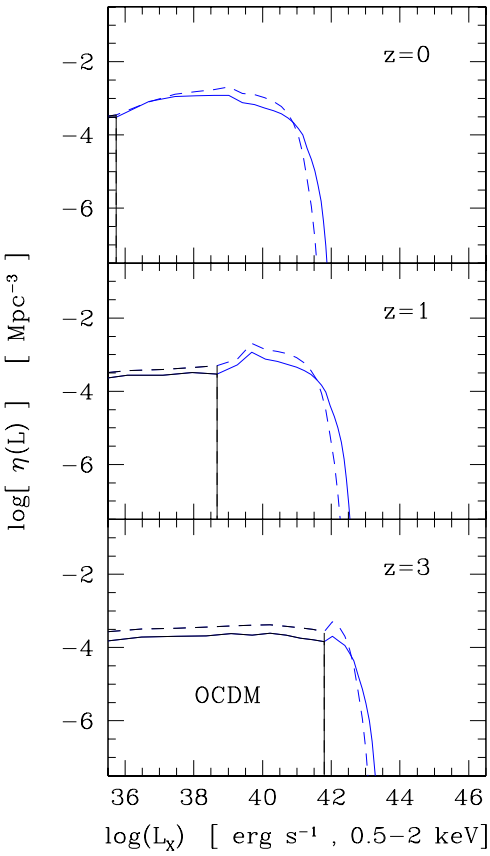

Fig. 16. The comoving galaxy X-ray luminosity function in the rest-frame frequency band 0.5–2 keV for the OCDM scenario. Same curves as in Fig. 15.

galaxies since an increasingly large fraction of these objects is cold. Moreover, the contribution of small galaxies (which have a low virial temperature T) is strongly suppressed by the factors $\exp(-h_P\nu/kT)$ which enter the X-ray luminosity (36).

As usual, the redshift evolution is smaller for the open universe (see Valageas & Schaeffer 1999) as the galaxy multiplicity function evolves more slowly (for the same reason as for the cluster multiplicity function). However, the cutoff $L_{Xf}(z)$ increases faster with z than for the SCDM case. This is due to the fact that the temperature attached to these galaxies (in particular T_f) is somewhat smaller for the low-density universe which implies that the factors $\exp(-h_P\nu/kT)$ are more sensitive to T_f and evolve faster with z. Note that the X-ray luminosity $L_{Xf}(z)$ is indeed lower for the open universe. As explained in Sect. 6.1.1 the cooling constraint plays a greater role at small redshift, as shown by the comparison between the "Hot" and "Cold" models. This implies that the difference between both scenarios is largest at $z = 0$. Note that even for the "Hot" model the high luminosity cutoff is stronger at lower z. This is due to the gradual decline with time of the mass of hot gas M_{hot} attached to these halos together with the larger Hubble time $t_H(z)$, see (45) and (42).

6.2. Quasar X-ray luminosity function

In addition to galaxies, groups and clusters, quasars are X-ray emitters. In fact, as we shall see in the next section their contribution to the X-ray flux is much larger than the galactic emission because of their harder radiation spectrum (which is roughly similar to a power-law as opposed to the black-body spectrum of stars). Thus, it is of interest to estimate the quasar source counts since they dominate at fluxes smaller than those corresponding to clusters. Moreover, it allows us to obtain a complete description of X-ray objects within the framework of a unified model. Indeed, since in our model QSOs correspond to galaxies where some gas is accreted by a central black hole the quasar luminosity function is derived from the galaxy multiplicity function. Hence it is fully consistent with the cluster and galaxy mass functions we obtained in the previous sections. We now briefly describe our model for quasars, which is similar to the one used in Valageas & Silk (1999a,b) to study the reheating and reionization history of the universe.

6.2.1. Quasar multiplicity function

First, we assume that the mass M_Q which is available to fuel the quasar is proportional to the sum of the mass of central gas M_{gc} and of stars which formed lately ΔM_s:

$$M_Q = F(M_{gc} + \Delta M_s). \tag{46}$$

Thus, at late times when most of the gas is consumed into stars the total mass of the black hole is $M_{BH} \sim F M_s$. We use $F = 0.005$ since observations from Magorrian et al. (1998) find that $M_{BH} \sim 0.005 M_{sph}$ where M_{sph} is the mass of the stellar bulge. From the model of star formation described in Valageas & Schaeffer (1999) we have:

$$M_{gc} = \left(1 + \frac{T_{SN}}{T}\right)^{-1} e^{-\lambda} M_b \tag{47}$$

and

$$\Delta M_s \equiv M_s \ \min\left(1, \frac{t_H}{M_s}\frac{dM_s}{dt}\right) = \lambda\, e^{-\lambda} M_b, \tag{48}$$

where M_b is the mass of baryons in the galaxy and as a function of our scaling parameter x

$$\lambda(x) = \frac{p}{\beta_d}\left(1 + \frac{T_{SN}}{T}\right)^{-1} \sqrt{\frac{(1+\Delta)_{gal}(x)}{(1+\Delta_c)}}. \tag{49}$$

Here $p/\beta_d \simeq 0.5$ is a parameter which enters the definition of the dynamical time, while $T_{SN} \sim 10^6$ K describes the ejection of gas by supernovae and stellar winds (see also Kauffmann et al. 1993). The coefficient λ measures the efficiency of star formation. Thus, small galaxies with $T \ll T_{SN}$ have $\lambda \ll 1$ because supernovae eject a large fraction of the gas out of the inner parts of the galaxy. Hence $M_{gc} \ll M_b$ and $\Delta M_s \sim M_s \ll M_b$ as seen in (47) and (48). On the other hand, massive old galaxies with a density contrast $\Delta_{gal} > \Delta_c$ have a small dynamical time, hence a small star formation time in our model. This leads to the factor $\sqrt{(1+\Delta)_{gal}}$ in (49). Hence they have $\lambda \gg 1$ and they have already consumed most of their gas, so that the quasar runs out of fuel, see (47) and (48). Next, if we note $f_{\rm Ed}$ the Eddington ratio we write the quasar luminosity $L_Q = f_{\rm Ed} L_{\rm Ed}$ as:

$$L_Q = f_{\rm Ed}\frac{M_Q\, c^2}{t_*} \quad \text{with} \quad t_* = 4.4\ 10^8 \text{yr}, \tag{50}$$

while the quasar life-time t_Q is:

$$t_Q = \frac{\epsilon_Q}{f_{\rm Ed}}\, t_*, \tag{51}$$

where $\epsilon_Q = 0.05$ is the quasar radiative efficiency. Finally, we write the quasar multiplicity function we would obtain without any scatter as:

$$\eta_Q(M_Q)\frac{dM_Q}{M_Q} = \lambda_Q\, \frac{t_Q}{t_M}\, \eta_g(M)\frac{dM}{M} \tag{52}$$

where $\eta_g(M)dM/M$ is the galaxy mass function obtained in Sect. 6.1. Here $t_M \sim t_H$ is the evolution time-scale of galactic halos of mass M defined by:

$$t_M^{-1} = \text{Max}\left(t_H^{-1}\ ,\ \frac{1}{\eta_g(M)}\,\frac{\partial}{\partial t}\eta_g(M)\right). \tag{53}$$

We use $\lambda_Q \sim 0.05$. Note that here we only have two free parameters $(f_{\rm Ed}F)$ and $(\lambda_Q \epsilon_Q / f_{\rm Ed})$ so that we could for instance use a larger $f_{\rm Ed}$ with a smaller F and larger λ_Q. Moreover, the properties of quasars show a significant scatter. For instance, Magorrian et al. (1998) find that the decimal logarithm of the ratio $F = M_{BH}/M_{sph}$ obeys a Gaussian distribution of mean -2.28 and standard deviation ~ 0.51. Hence we assume here that the actual luminosity L_{Qscat} of QSOs is related to the luminosity L_Q defined in (50) by:

$$L_{Qscat} = e^u\, L_Q \quad , \quad P(u) = \frac{1}{\sqrt{2\pi\sigma_u^2}}\, e^{-u^2/2\sigma_u^2} \tag{54}$$

where $P(u)du$ is the probability distribution of the random variable u. Thus, we assume $P(u)$ to be a Gaussian of width $\sigma_u = 1.15$ (resp. $\sigma_u = 1$) for the SCDM (resp. OCDM) scenario. Note that $\sigma_u = 1.15$ corresponds to the scatter observed by Magorrian et al. (1998) for the ratio F. Although part of this scatter may be due to the observational noise, which would decrease σ_u, the random variable u also describes the scatter of the other properties of quasars like the Eddington ratio $f_{\rm Ed}$. Then, we obtain the final quasar luminosity function from (52) and (54):

$$\eta_{Qscat}(L_{Qscat}) = \int_{-\infty}^{\infty} du\ P(u)\ \eta_Q\left(L_{Qscat}\ e^{-u}\right). \tag{55}$$

Since observations suggest that the Eddington ratio $f_{\rm Ed}$ increases with the luminosity L_Q (Padovani 1989; Wandel 1998) we use the parameterization:

$$f_{\rm Ed} = \text{Min}\left[2\ ,\ \left(\frac{L_{\rm Ed}}{10^{47}\ \text{erg s}^{-1}}\right)^{0.33}\right] \tag{56}$$

in order to be consistent with the data obtained by Padovani (1989). This author finds that most of the observed dependence of $f_{\rm Ed}$ on redshift is accounted for by the dependence on luminosity (low z quasars are fainter than high z QSOs) hence we do not add any explicit dependence on redshift in our model (56). However, in order to estimate the influence of these various parameterizations we also consider for the B-band luminosity functions displayed in Fig. 17 and Fig. 18 the following two alternative models (A) and (B) with:

$$\text{(A)}: \ f_{\rm Ed} = 1 \tag{57}$$

and

$$\text{(B)}: \ t_Q = \text{Max}\left(2\times 10^8\ (1+z)^{-1.5}\ \text{yr}\ ,\ \frac{\epsilon_Q}{2}\ t_*\right). \tag{58}$$

Thus, model (A) corresponds to a constant Eddington ratio of unity while model (B) corresponds to an accretion time which is roughly proportional to the Hubble time (with a lower bound so that $f_{\rm Ed} \leq 2$). Finally, in order to point out the importance of correctly identifying the galactic halos we also display in Fig. 17 and Fig. 18 the "model" (C) where all halos are defined by the virialization constraint as in (41). Of course, as in Sect. 6.1.1 we only show this "model" for illustrative purposes since it is not valid for massive halos. However, note that usual analytic

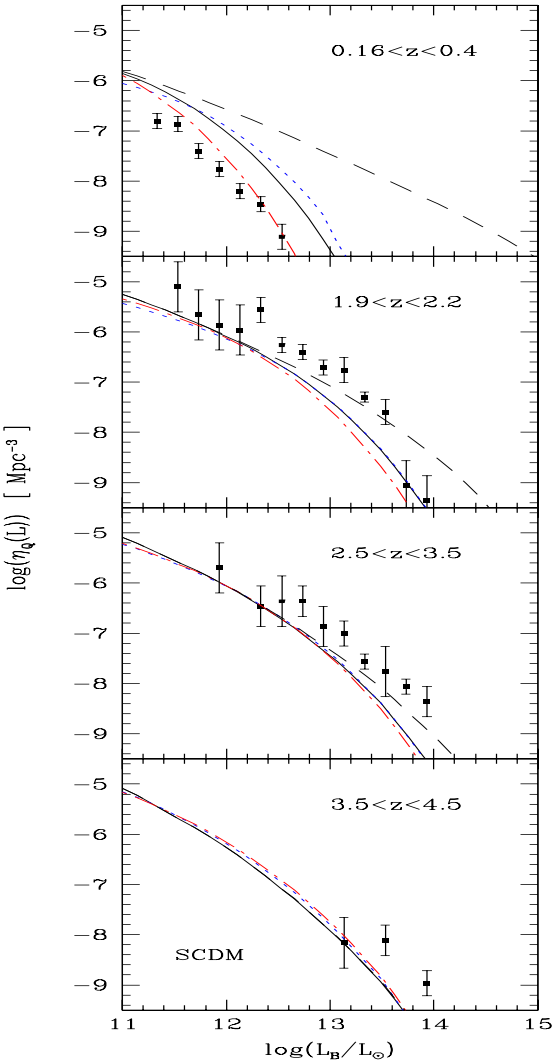

Fig. 17. The comoving quasar B-band luminosity function for the SCDM case. The data points are observations from Pei (1995). The solid lines correspond to our fiducial model, the dotted lines to (A), the dot-dashed lines to (B) and the dashed lines to (C), see main text.

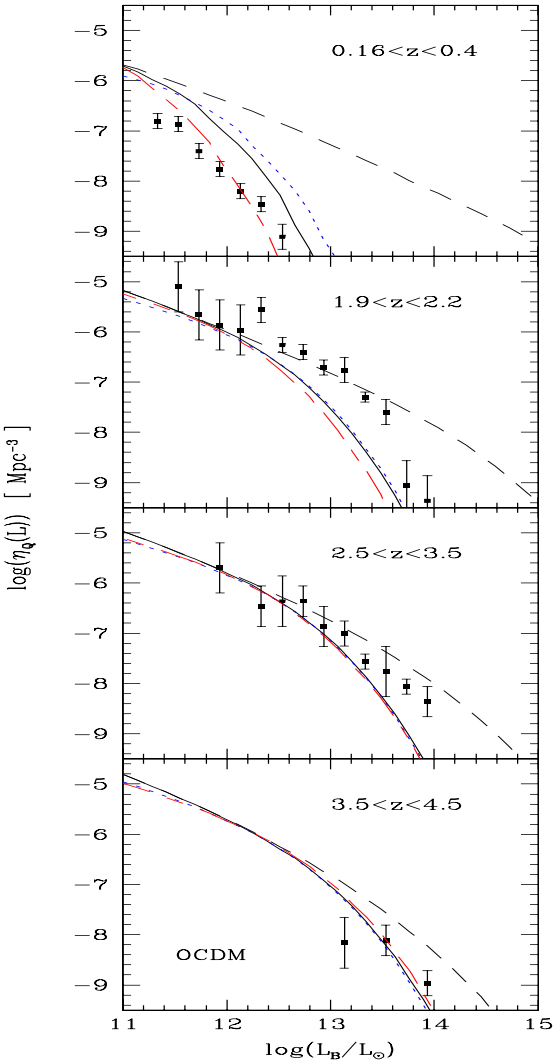

Fig. 18. The comoving quasar B-band luminosity function for the OCDM case as in Fig. 17.

models based on the PS approach (e.g., Haiman & Menou 1999) define halos as in (C).

We show the B-band quasar luminosity functions that we obtain in Fig. 17 and Fig. 18 for both SCDM and OCDM cosmologies. First, we note that our result (solid lines) agree reasonably well with observations over the whole range $0 < z < 4.5$. Moreover, we can check that both models (A) (dotted lines) and (B) (dot-dashed lines) are quite close to our fiducial model. Thus, although our model is very crude our predictions should provide a reasonable estimate of the quasar multiplicity since they are not too sensitive to details. Note, however, that the model (B) shows a slightly better agreement with observations as it leads to a stronger decrease of the quasar number density at low z. This is due to the redshift evolution of the quasar life-time t_Q which implies a smaller Eddington ratio $f_{\rm Ed}$ at low z. On the other hand, we can clearly see that the "model" (C) fails at low redshift $z < 2$. Indeed, since it counts groups or clusters as one halo it predicts a significant number of huge quasars, which is inconsistent with observations. Of course, at high redshift where the cooling condition (first constraint in (39)) plays no role the "model" (C) superposes onto our model (56) since all galaxies are defined by the usual density threshold $\Delta_c(z)$.

Thus, one cannot use the (standard) PS prescription to obtain the QSO luminosity function at low z. Hence one should be careful about the use of the PS mass function to derive the redshift evolution of quasar properties from the observed luminosity function. For instance, while Haiman & Menou (1999) find that this procedure implies that the Eddington ratio $f_{\rm Ed}$ or the mass ratio F must drop by a factor ~ 100 at low z between $0 \lesssim z \lesssim 3$ (which would steepen the dashed curves shown in the upper panel in Fig. 17 and Fig. 18), they note that a possible "solution" would be to correct the halo mass function in order to make sure that one counts galactic halos and not clusters. Indeed, our results show that the correct procedure (i.e. identifying galactic halos) provides by itself a reasonable agreement with observations, without any additional ad-hoc redshift depen-

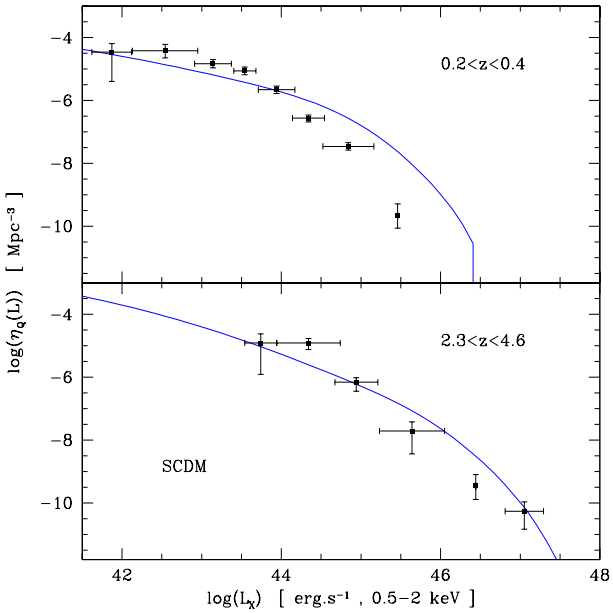

Fig. 19. The comoving quasar X-ray luminosity function in the frequency band 0.5–$2\,\mathrm{keV}$ for the case $\Omega_\mathrm{m} = 1$. The data points are observations from Miyaji et al. (1998).

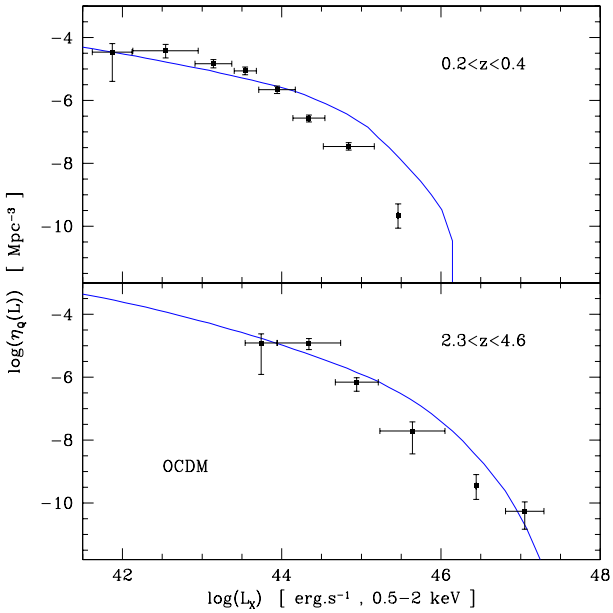

Fig. 20. The comoving quasar X-ray luminosity function in the frequency band 0.5–$2\,\mathrm{keV}$ for the OCDM scenario.

dence. It could be tempting to introduce a redshift dependence of the form (58), to improve somewhat the fit to observations. Nevertheless, we consider the present models too crude to allow one to draw such conclusions from the observations: such a mouve would plug theoretical inaccuracies into an artificial "observed" evolution of (58) with redshift. Note however that such an evolution with redshift may exist.

6.2.2. Quasar X-ray emission

From the quasar multiplicity function we obtain the X-ray source counts which are identified as QSOs as in (38). We assume that the quasar spectrum is locally a power-law $L_\nu \propto \nu^{-1.5}$ around $\nu_1 = 1\,\mathrm{keV}$, normalized by $(L_1/L_{bol}) = 0.028$ with $L_1 = \nu_1 L_\nu(\nu_1)$. We present in Fig. 19 and Fig. 20 the comoving quasar luminosity function we obtain for both SCDM and OCDM cosmologies. The frequency band 0.5–$2\,\mathrm{keV}$ corresponds to the observed spectrum (i.e. light was emitted between $0.5(1+z)$ and $2(1+z)\,\mathrm{keV}$). We see that we obtain a reasonable agreement with observations from Miyaji et al. (1998), both at low redshift $z \sim 0.3$ and high redshift $z \sim 3.5$. This could be expected from the results of Fig. 17 and Fig. 18 for the B-band luminosity function.

6.3. Galaxy and quasar versus group and cluster counts

From the X-ray luminosity functions obtained in the previous sections we can derive the surface density on the sky of sources brighter than an X-ray flux limit S_X, taking into account the contribution from galaxies as well as from QSOs, groups and clusters. We show our results for the scaling model in Fig. 21. First, we note that the prediction of the "Hot" model for the galaxy counts is much larger than for the "Cold" scenario, especially for the low-density cosmology. This could be expected from the comparison of Fig. 15 with Fig. 16. Thus, in the "Hot" scenario the contribution from individual galaxies dominates over groups and clusters at $S_X \lesssim 10^{-16}\,\mathrm{erg\,s^{-1}\,cm^{-2}}$ while in the "Cold" scenario this only holds for $S_X \lesssim 10^{-18}\,\mathrm{erg\,s^{-1}\,cm^{-2}}$ for the SCDM case and for even smaller fluxes for the OCDM cosmology. This is due to the much lower cutoff L_{Xf} in the OCDM scenario, as seen in Fig. 15 and Fig. 16. Of course, the characteristic fluxes of galaxies are much smaller than for clusters because of their smaller mass and temperature. Moreover, a significant part of the gas of bright galaxies has been able to cool due to their higher redshift of formation. This leads to the sharp high-flux cutoff of the galaxy counts as compared with the group and cluster counts, even for the "Hot" model. However, at low S_X galaxies provide a larger contribution than groups because they are much more numerous.

In the "Cold" scenario, the observation of these X-ray emitting galaxies would provide *a direct signature of galaxy formation and of the associated cooling process*. Bright galaxies already start to appear at $S_X \sim 10^{-16}\,\mathrm{erg\,s^{-1}\,cm^{-2}}$, typically one per square degree, and are within the AXAF sensitivity limits[1]. In our model (see Valageas & Schaeffer 1999), such bright galaxies typically correspond to a virial temperature of $10^7\,K$ and a baryon mass of $2.3 \times 10^{11} M_\odot$. They are just forming at $z = 3$, with an X-ray luminosity of $1.5 \times 10^{43}\,\mathrm{erg\,s^{-1}}$ over a time of 1.4×10^9 years. However, in the "Hot" scenario most X-ray emitting galaxies would have already seen a large part of their gas content cool and the observed luminosity would arise from a diffuse hot component, left-over from the last merging event or replenished by supernovae, which only contains

[1] We are indebted to R. Mushotzky for a discussion of this point.

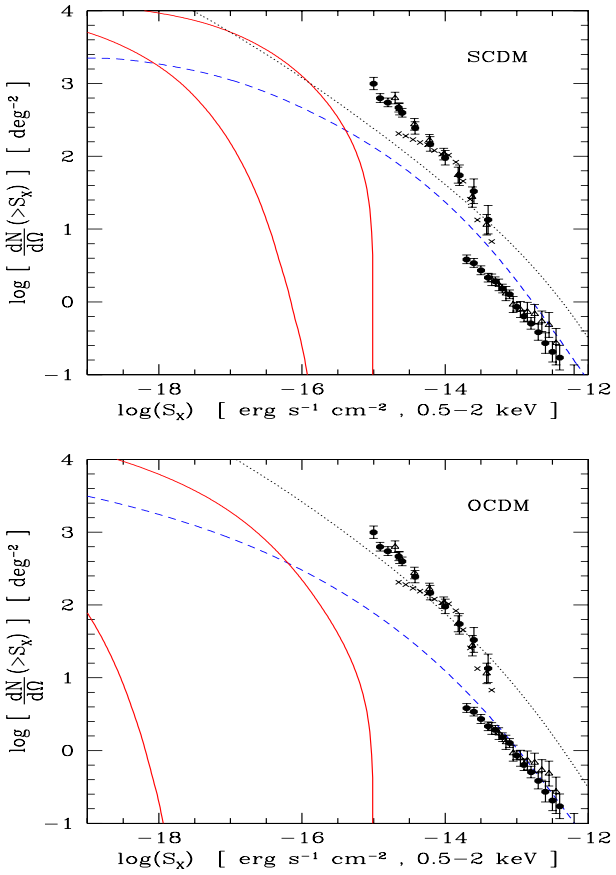

Fig. 21. *Upper panel*: the number of sources per square degree brighter than an X-ray flux limit S_X for the case $\Omega_{\rm m} = 1$. The solid lines correspond to galaxies for the "Hot" model (upper curve) and the "Cold" model (lower curve). The dashed line corresponds to groups and clusters. The dotted line shows the quasar number counts. We only display the scaling model. The data points for quasars are from Hasinger et al. (1998) (disks for the 1112 ksec PSPC and triangles for the 207 ksec HRI) and McHardy et al. (1998) (crosses). The data points for clusters are as in Fig. 13. *Lower panel*: same curves for an open universe with $\Omega_{\rm m} = 0.3$.

a small fraction of the total baryonic mass. In any case, it is clear that observations (and even the lack of galaxy detections at $S_X \sim 10^{-16}\,{\rm erg\,s^{-1}\,cm^{-2}}$) would provide very interesting informations on galaxy formation and evolution. As we noted above, however, due to theoretical and observational ambiguities the most relevant curve is probably the sum of both contributions from galaxies and groups. Thus, we see that the predictions obtained for both cosmologies are similar.

On the other hand, because of their harder radiation spectrum, quasars provide an important contribution to the X-ray source counts, which actually dominates over the whole range $10^{-18} < S_X < 10^{-12}\,{\rm erg\,s^{-1}\,cm^{-2}}$. We note that although we recover the right abundance of AGN source counts at high luminosities $S_X \sim 10^{-14}\,{\rm erg\,s^{-1}\,cm^{-2}}$ we somewhat underestimate the number of low luminosity objects $S_X \sim 10^{-15}\,{\rm erg\,s^{-1}\,cm^{-2}}$. This may suggest that a more detailed model of QSOs is needed in order to match exactly the observations. On the other hand, we note that McHardy et al. (1998) find that at low fluxes a new population of sources appears, which consists of narrow emission lines galaxies which could partly correspond to starburst galaxies, which we did not specifically include in our model.

7. Summary and conclusion

We have examined the predictions of the *scaling model* for the number of X-ray emitting objects as a function of redshift. This approach gives the multiplicity of non-linear structures directly from the non-linear density field and should be considered as an improvement over the PS approximation. This model gives more precise counts and can also be used for any density contrast, both much larger tha n the usual value of 200 as well as much smaller. It also solves the hierarchy (cloud-in-cloud) problem and allows us to describe structures embedded within other virialized condensations. Thus we can simultaneously describe galaxies (and quasars) as well as galaxy clusters.

For the cluster temperature and X-ray luminosity distributions, the counts obtained in this way typically differ by a factor of two from the PS approximation, but the differences may reach an order of magnitude for extreme cases (very large or very small objects). With an initial CDM spectrum that is normalized in the same way as in the numerical simulations that reproduce the same data, the scaling model reproduces the currently available observations, while the PS approximation does not (the latter would, provided the normalization of the power spectrum is modified, with however a different modification depending on the observations to be reproduced). The evolution with redshift is different too, for reasons that are well understood. The counts for $T > 5\,{\rm keV}$, for instance, peak at $z = 0.4$ rather than $z = 0.2$ for $\Omega_{\rm m} = 1$, with a much larger normalization.

This allows a more accurate estimation of the Sunyaev-Zel'dovich distorsion parameter y along a given line of sight (summing over the contribution of clusters). For the same CDM initial conditions as above, we get $\langle y \rangle = 2 \times 10^{-6}$ that induces fluctuations $\langle \delta y^2 \rangle^{1/2} = 10^{-6}$ in the CMB for $\Omega_{\rm m} = 0.3$, and values which are a factor of two smaller in a critical density universe, the bulk of the contribution arising from clusters at $z < 1$.

Then, we have shown that models of the intra-cluster medium which include a characteristic temperature $T_{ad} \sim 0.4\,{\rm keV}$ reproduce the main features of the observed temperature - X-ray luminosity relation, independently of the details of the models. This provides a robust estimate of the luminosity function which is seen to show a very weak dependence on redshift.

Next, we have recalled how to build a model for galaxies and quasars in a way that is consistent with the description of clusters and of the underlying density field. In particular, we have pointed out the advantages of our approach which allow us to study these high-density objects which cannot be dealt with by the standard PS prescription. Thus, we show that the analysis of the observed QSO luminosity function in the light of the PS mass function leads to discrepancies and to erroneous

conclusions due to the intrinsic limitations of this theoretical approach. On the other hand, thanks to its more extended range of applications, our method can be meaningfully used to study these objects and it provides a much better agreement with the data. This also holds for the galaxy luminosity function, for the same physical reasons.

Finally, we have taken advantage of being able to use the same basic model to draw a global description of the X-ray emission from all structures. Thus, we find that quasars dominate the X-ray source counts over the available range of fluxes. Clusters and groups provide a non-negligible contribution ($\sim 1/5$ of the quasar counts) over the same range. On the other hand, at low fluxes $S_X \sim 10^{-16}\,\mathrm{erg\,s^{-1}\,cm^{-2}}$ one starts to get access to individual galaxies, especially for a critical density universe. For the OCDM scenario, this only occurs if there is inhomogeneous cooling so that a hot diffuse gaseous component remains in the galactic halo while gradually losing mass in the form of cold gas (otherwise, if there is no such hot gas, galaxies only appear for $S_X \sim 10^{-18}\,\mathrm{erg\,s^{-1}\,cm^{-2}}$ in this OCDM cosmology). These objects, that were more luminous in the past and start appearing in deep enough surveys, are undoubtedly a new challenge. In particular, they should be accessible with the current sensitivity of AXAF. Thus, observations of X-ray emitting galaxies (or the lack of detection) will provide interesting information on galaxy evolution. They will constrain the amount of hot gas within galactic halos (which in turn could give some constraints on the feedback from supernovae and the infall from the IGM) and especially uncover some massive galaxies while they are just being formed.

References

Arnaud M., Evrard A.E., 1999, MNRAS 305, 631
Balian R., Schaeffer R., 1989, A&A 220, 1
Barbosa D., Bartlett J.G., Blanchard A., Oukbir J., 1996, A&A 314, 13
Bardeen J., Bond J.R., Kaiser N., Szalay A., 1986, ApJ 304, 15
Bernardeau F., Schaeffer R., 1991, A&A 220, 23
Bernardeau F., Schaeffer R., 1992, A&A 225, 1
Bernardeau F., Schaeffer R., 1999, A&A 349, 697
Bouchet F.R., Schaeffer R., Davis M., 1991, ApJ 383, 19
Burns J.O., Ledlow M.J., Loken C., et al., 1996, ApJ 467, L49
Cavaliere A., Menci N., Tozzi P., 1997, ApJ 484, L21
Cavaliere A., Menci N., Tozzi P., 1999, MNRAS 308, 599
Cole S., Lacey C., 1996, MNRAS 281, 716
Colombi S., Bernardeau F., Bouchet F.R., Hernquist L., 1997, MNRAS 287, 241
Davis M., Efstathiou G.P., Frenk C.S., White S.D.M., 1985, ApJ 292, 371
de Bernardis P., Ade P.A.R., Bock J.J., 2000, Nat 404, 955
Ebeling H., Edge A.C., Fabian A.C., Allen S.W., Crawford C.S., 1997, ApJ 479, L101 Edge A.C., Stewart G.C., Fabian A.C., Arnaud K.A., 1990, MNRAS 245, 559
Eke V.R., Cole S., Frenk C.S., 1996, MNRAS 282, 263
Eke V.R., Navarro J.F., Frenk C.S., 1998, ApJ 503, 569
Ellis R.S., Colless M., Broadhurst T., Heyl J., Glazebrook K., 1996, MNRAS 280, 235
Evrard A.E., Henry J.P., 1991, ApJ 383, 95
Evrard A.E., Metzler C.A., Navarro J.F., 1996, ApJ 469, 494
Fixsen D.J., Cheng E.S., Gales J.M., et al., 1996, ApJ 473, 576
Governato F., Babul A., Quinn T., Baugh C.M., Katz N., Lake G., 1999, MNRAS 307, 949
Gross M.A.K., Somerville R.S., Primack J.R., Holtzman J., Klypin A., 1998, MNRAS 301, 81
Haiman Z., Menou K., 2000, ApJ 531, 42
Hasinger G., Burg R., Giacconi R., et al., 1998, A&A 329, 482
Henry J.P., Arnaud K.A., 1991, ApJ 372, 410
Henry J.P., 1997, ApJ 489, L1
Jones L.R., Scharf C., Ebeling H., et al., 1998, ApJ 495, 100
Kaiser N., 1986, MNRAS 222, 323
Kauffmann G., White S.D.M., Guiderdoni B., 1993, MNRAS 264, 201
Lloyd-Davies E.J., Ponman T.J., Cannon D.B., 2000, MNRAS 315, 689
Loveday J., Peterson B.A., Efstathiou G., Maddox S.J., 1992, ApJ 390, 338
Magorrian J., Tremaine S., Richstone D., et al., 1998, AJ 115, 2285
Mc Hardy I.M., Jones L.R., Merrifield M.R., et al., 1998, MNRAS 295, 641
Miyaji T., Hasinger G., Schmidt M., 1998, Proceedings of: Highlights in X-ray Astronomy. astro-ph 9809398
Monaco P., Salucci P., Danese L., 2000, MNRAS 311, 279
Moore B., Ghigna S., Governato F., Lake G., Quinn T., Stadel J., Tozzi P., 1999a, ApJ 524, L19
Moore B., Quinn T., Governato F., Stadel J., Lake G., 1999b, MNRAS 310, 1147
Munshi D., Bernardeau F., Melott A.L., Schaeffer R., 1999, MNRAS 303, 433
Mushotzky R.F., Scharf C.A., 1997, ApJ 482, L13
Navarro J.F., Frenk C.S., White S.D.M., 1995, MNRAS 275, 720
Navarro J.F., Frenk C.S., White S.D.M., 1996, ApJ 462, 563
Nulsen P.E.J., 1986, MNRAS 221, 377
Nulsen P.E.J., 1998, MNRAS 297, 1109
Oukbir J., Blanchard A., 1992, A&A 262, L21
Oukbir J., Blanchard A., 1997, A&A 317, 1
Padovani P., 1989, A&A 209, 27
Peacock J.A., Heavens A.F., 1990, MNRAS 243, 133
Peacock J.A., Dodds S.J., 1996, MNRAS 280, L19
Pei Y.C., 1995, ApJ 438, 623
Ponman T.J., Bourner P.D., Ebeling H., Bohringer H., 1996, MNRAS 283, 690
Ponman T.J., Cannon D.B., Navarro J.F., 1999, Nat 397, 135
Press W.H., Schechter P., 1974, ApJ 187, 425
Rosati P., Della Ceca R., Norman C., Giacconi R., 1998 ApJ 492, L21
Sarazin C.L., 1988, X-ray emissions from clusters of galaxies. Cambridge Astrophysics Series, Cambridge University Press
Schaeffer R., 1984, A&A 134, L5
Schaeffer R., 1985, A&A 144, L1
Schaeffer R., Silk J., 1988, A&A 203, 273
Sunyaev R.A., Zel'dovich Y.B., 1972, Comm. Astrophys. Space Phys. 4, 173
Teyssier R., Chieze J.-P., Alimi J.-M., 1997, In: Durret F., et al. (eds.) Proc.: A new vision of an old cluster. France, astro-ph 9710010
Valageas P., Schaeffer R., 1997, A&A 328, 435 (VS)
Valageas P., Schaeffer R., 1999, A&A 345, 329
Valageas P., Silk J., 1999a, A&A 347, 1
Valageas P., Silk J., 1999b, A&A 350, 725
Valageas P., Schaeffer R., Silk J., 1999, A&A 345, 691
Valageas P., 2000, A&A 356, 771
Valageas P., Lacey C., Schaeffer R., 2000a, MNRAS 311, 234

Valageas P., Schaeffer R., Silk J., 2000b, submitted to A&A, astro-ph 0001207
Wandel A., 1998, In: Gaskell C.M., et al. (eds.) Structure and kinematics of quasar broad line regions. ASP Press, San Francisco, astro-ph 9808171
Waxman E., Miralda-Escude J., 1995, ApJ 451, 451
Wu K.K.S., Fabian A.C., Nulsen P.E.J., 1999, submitted to MNRAS, astro-ph 9907112
Zucca E., Zamorani G., Vettolani G., et al., 1997, A&A 326, 477